Photoluminescence of Chalcopyrite Tellurides

ANDRI JAGOMÄGI

Tallinn 2006

TALLINN UNIVERSITY OF TECHNOLOGY
Department of Materials Science

Dissertation was accepted for the defence of the degree of Doctor of Philosophy in Natural and Exact Sciences on 20th of October, 2006.

Supervisor: Prof. Jüri Krustok, Department of Materials Science, Tallinn University of Technology

Opponents: dr. Heikki Collan, Helsinki University of Technology, Optoelectronics Laboratory, Tietotie 3, 02150 Espoo, FINLAND

dr. Raivo Jaaniso, Tartu Ülikool, Füüsika Instituut, Riia 142, 51014 Tartu

Defence: 30th of November, 2006, at 12.00
Lecture hall: V-103
Tallinn University of Technology, Ehitajate tee 5, Tallinn

Declaration: Hereby I declare that this doctoral thesis, my original investigation and achievement, submitted for the doctoral degree at Tallinn University of Technology, has not been submitted for any degree or examination.

Andri Jagomägi

Kalkopüriitsete telluriidide fotoluminestsents

ANDRI JAGOMÄGI

Tallinn 2006

The thesis is based on the following papers:

A. Jagomägi, J. Krustok, J. Raudoja, M. Grossberg, I. Oja, M. Krunks, M. Danilson, Photoluminescence and Raman spectroscopy of polycrystalline $AgInTe_2$, *Thin Solid Films*, v. 480-481, pp. 246-249 (2005)

A. Jagomägi, J. Krustok, J. Raudoja, M. Grossberg, M. Danilson, M.Yakushev, Photoluminescence studies of heavily doped $CuInTe_2$ crystals, *Physica B* **337,** pp. 369-374 (2003)

A. Jagomägi, J. Krustok, J. Raudoja, M. Grossberg, M. Danilson, Deep and edge photoluminescence emission of $CuInTe_2$, *Physica Status Solidi* **237,** R3-R5 (2003)

J. Krustok, **A. Jagomägi**, M. Grossberg, J. Raudoja, and M. Danilson, Photoluminescence properties of polycrystalline $AgGaTe_2$, *Solar Energy Materials and Solar Cells*,. v. 90, No. 13, pp. 1973-1982 (2006).

A. Jagomägi, J. Krustok, M. Grossberg, M. Danilson, and J. Raudoja, Deep defect related photoluminescence in heavily doped $CuGaTe_2$ crystals, *Physica Status Solidi (a)*, v.203, No. 5, pp. 949-955, (2006).

Table of contents

1 Abstract

Photoluminescence of chalcopyrite tellurides

Photoluminescence is a sensitive method for studies of defect structure of semiconductor materials. The studied chalcopyrite telluride compounds belong to the I-III-VI$_2$ group of semiconductors. These materials have many novel applications, including a potential of being an absorber material in thin film solar cells. The studied materials include CuInTe$_2$, CuGaTe$_2$, AgInTe$_2$, and AgGaTe$_2$.

The results of the experiments were multifarious in terms of the features of the photoluminescence spectra. Nevertheless, the crystal structure and properties of all these materials are very similar, the photoluminescence spectra had shapes from broad asymmetric bands, which are characteristic of heavily doped semiconductors, to narrow excitonic peaks with phonon replicas that implies a rather good crystal quality.

The photoluminescence spectra of single crystalline CuInTe$_2$ and their dependence on the temperature and excitation power were measured. At 10 K an asymmetric broad peak at 0.98 eV was observed. The photoluminescence peak position did not depend on the excitation power, but had a characteristic dependence on the sample temperature. Our computer simulations proved that this behavior is in good compliance with the Shklovskij/Efros model of heavily doped semiconductors with spatially varying potential fluctuations. Therefore, the photoluminescence band was attributed to the band-to-impurity type recombination and the corresponding level to the single acceptor at 70 meV, which is most probably caused by a copper vacancy.

Photoluminescence studies of polycrystalline CuInTe$_2$ showed three edge (1.041 eV, 1.030 eV, and 1.019 eV) and two deep level (0.999 eV, and 0.957 eV) emission bands at 11K. The excitation intensity and temperature dependencies of photoluminescence spectra were recorded. As possible band sources one excitonic and four band-to-defect recombination mechanisms are proposed in this thesis.

The photoluminescence spectra of polycrystalline AgGaTe$_2$ showed two emission regions centred at 1.32 eV and 0.8 eV. The first region appears near the bandgap energy and comprises three bands that are identified by the theory of heavily doped semiconductors as band-to-band (1.337 eV), band-to-tail (1.317 eV) and band-to-impurity (1.287 eV) recombination.

CuGaTe$_2$ samples very often exhibit optical and electrical properties of heavily doped semiconductors. The deep photoluminescence region observed (0.8 - 1.3 eV) consists of two peaks. One of them is located at 0.955 eV and has been reported before. Another, a totally new band was discovered at 1.14 eV. The low-temperature j-shift of both bands was detected. Also, rather significant blue shift with the increasing temperature was noticed. It is proposed that both bands consist of two recombination channels. At low temperatures tail-to-impurity recombination dominates. As the temperature increases, the tail-to-impurity recombination transforms into band-to-impurity recombination.

The last chalcopyrite compound that we studied was polycrystalline $AgInTe_2$. The spectra showed three bands. The first band has the maximum at 1.023 eV and it has one LO-phonon replica with the energy shift of 25 meV. The second band has the maximum at 0.959 eV and two phonon replicas with the same 25 meV LO-phonon energy. The third broad band has the maximum at 0.741 eV. The dependence of the spectra on the temperature and the excitation power were recorded. According to the observed j-shift and thermal quenching the 0.959 eV band can be assigned to a donor-acceptor pair recombination with the activation energy of 35 meV. The intensities of the first and the third band were not sufficient to record their temperature or laser power dependencies. Nevertheless, we propose that the first one has excitonic origin and the third one has been caused by some deep defect state.

2   Kokkuvõte

Fotoluminestsents on tundlik ning suhteliselt lihtne meetod pooljuhtide defektstruktuuri uurimiseks. Käesoleva töö eesmärgiks oli uurida I-III-IV$_2$ gruppi kuuluvate telluriidide fotoluminestsentsi omadusi. Nendel materjalidel on terve rida kaasaegseid rakendusi, millest kõige tuntum on ehk nende kasutamine päikesepatareide absorberkihina. Antud töös uurisime nelja pooljuhtmaterjali: CuInTe$_2$, CuGaTe$_2$, AgInTe$_2$ ja AgGaTe$_2$.

Eksperimentide tulemused olid väga mitmekülgsed. Mõõdetud spektrites leidus laiu fotoluminestsentsribasid, mis on iseloomulikud tugevalt legeeritud pooljuhtidele. Samuti leidus peenstruktuurseid foononkordustega ribasid, mis on iseloomulikud pigem hea kvaliteediga puhastele kristallidele.

Monokristalse CuInTe$_2$ fotoluminestsentsspekter temperatuuril 10 K koosnes ühest laiast ebasümmeetrilisest ribast, mille haripunkt asus 0,98 eV juures. Selle riba kuju ega asukoht ei muutunud seoses ergastusvõimsuse muutmisega, samas näitas ta tugevalt legeeritud pooljuhile iseloomulikku käitumist seoses temperatuuri muutusega. Meie poolt läbi viidud arvutisimulatsioon tõestas, et selline käitumine on heas kooskõlas Shklovskij ning Efrose poolt välja töötatud tugevalt legeeritud pooljuhtide fotoluminestsentsi mudeliga. Tuginedes antud mudelile õnnestus meil tõestada, et detekteeritud kiirgusriba on tingitud tsoon-defekt rekombinatsioonist. Kaasatud defektitaseme aktivatsioonienergia on 70 meV ning tõenäoliselt on see põhjustatud vase vakantsi poolt.

Polükristalse CuInTe$_2$ uurimisel avastasime uue fotoluminestsentsriba, mille maksimumi energia asus 0,957 eV juures. Sellist kiirguskanalit antud materjalis pole keegi varem kirjeldanud. Spektrite temperatuursõltuvuste analüüs näitas, et selle kanali aktivatsioonienergia on 103 meV. See tulemus langeb hästi kokku varem avaldatud teoreetilise tööga, kus on pakutud ühe võimliku aktseptortaseme aktivatsioonienergiaks 120 meV. Antud avastus tõestab, et meie poolt kasutatud kasvatusmeetodiga on võimalik tekitada aktseptordefekte milleks on kas võrevaheline telluur või asendusdefekt, kus vase aatom on indiumi koha peal.

Polükristalse AgGaTe$_2$ fotoluminestsentsi spektri interpreteerimisel vaatasime kriitiliselt üle varem tehtud tööd ning andsime uue teoreetilise seletuse nende kristallide äärekiirgusele. Varem avaldatud eksitonilistele kiirgusallikatele pakkusime alternatiivi välja tugevalt legeeritud pooljuhtides esinevad rekombinatsioonimehhanismid nagu tsoon-tsoon, tsoon-tsoonisaba ning tsoon-defekt rekombinatsioonid. Meie interpretatsioon põhineb ribade temperatuursõltuvuse analüüsil.

Ka CuGaTe$_2$ kristallidel on tihti tugevalt legeeritud pooljuhtide omadused. Seda kinnitas fotoluminestsentsspektrite analüüs koos arvutisimulatsioonidega. Arvutil koostatud mudel toetas ideed, et kahe vaadeldud riba (1,14 eV ning 0,955 eV) tekkimine on seotud üleminekutega tsooni tasemelt defektitasemele. Madalatemperatuurse spektri sõltuvus ergastusvõimsusest näitas mõlema riba puhul nihkumist kõrgemate energiate suunas ergastusvõimsuse kasvamisel. Samasugune tendents ilmnes ka temperatuuri

kasvades konstantsel ergastusvõimsusel. Selline käitumine on kooskõlas mudeliga, milles mõlemad ribad koosnevad tegelikult kahest rekombinatsiooni kanalist. Madalatel temperatuuridel domineerib tsoonisaba-defekt üleminek. Kõrgematel temperatuuridel domineerib aga tsoon-defekt üleminek.

AgInTe$_2$ fotoluminestsentsi kohta oli varem kirjanduses avaldatud ainult üks artikkel, kus kirjeldati ühte laia kiirgusriba 0,7 eV juures. Meil õnnestus detekteerida ka AgInTe$_2$ äärekiirgus, mis koosnes peenstruktuursest spektrist. äärekiirguse analüüs näitas, et meil on esimesel juhul tegu donor-aktseptor paari ning teisel juhul eksitonilise rekombinatsiooniga.

3 Introduction

3.1 Chalcopyrite semiconductors

Chalcopyrite tellurides belong to the group of I-III-VI$_2$ semiconductors. Elements that form chalcopyrite semiconductor materials are highlighted in Table 1.1. Altogether, there are 36 types of chalcopyrite ternary semiconductors available. Half of them belong to the I-III-VI$_2$ family while the rest of them form II-IV-V$_2$ family. Among 18 former ones, only 6 are tellurides. Those chalcopyrite tellurides are **CuAlTe$_2$**, **CuGaTe$_2$**, **CuInTe$_2$**, **AgAlTe$_2$**, **AgGaTe$_2$**, and **AgInTe$_2$**. The name "**chalcopyrite**" comes from the naturally occurring copper iron sulfide mineral CuFeS$_2$, which crystallizes in the tetragonal system.

The chalcopyrite semiconductors have many unique optical, magnetic, and electrical properties that raise not only fundamental interest, but also have a great potential in technological applications. For example, in II-IV-V$_2$ family, **room-temperature ferromagnetism** has been observed [1,2]. This phenomenon that combines electrical transport and magnetism is required in electronics that is based on spin-related effects. Manganese doped CdGeP$_2$ is one of the promising candidates for this application.

Table 1.1. Periodic table of semiconductor-forming elements. Highlighted elements form I-III-VI$_2$ (white background) and II-IV-V$_2$ (grey background) chalcopyrite semiconductor structures.

I	II	III	IV	V	VI	VII	VIII			0
H										He
Li	Be	B	C	N	O	F				Ne
Na	Mg	Al	Si	P	S	Cl				Ar
K	Ca	Sc	Ti	V	Cr	Mn	Fe	Co	Ni	Co
Cu	Zn	Ga	Ge	As	Se	Br				Kr
Rb	Sr	Y	Zr	Nb	Mo	Tc	Ru	Rh	Pd	
Ag	Cd	In	Sn	Sb	Te	I				Xe
Cs	Ba		Hf	Ta	W	Re	Os	Ir	Pt	
Au	Hg	Ti	Pb	Bi	Po	At				Rn

Another feature of chalcopyrite semicondutcors is their **nonlinear optical properties** that come from their relatively large birefringence, which is caused by their built-in lattice compression [3]. This allows one to use them as optical frequency convertors [4]. Namely, ZnGeP$_2$, CdGeAs$_2$, AgGaS$_2$, and AgGaSe$_2$ are considered as high potential materials for frequency conversion. AgGaS$_2$ and AgGaSe$_2$ have already been commercialized as nonlinear optical crystals in the infrared region [5].

Because of their high optical absorption coefficient ($>10^4$ cm^{-1}) and near-optimum direct badgap value, many copper based chalcopyrite materials (Cu-

III-VI$_2$) with bandgaps between 1.0 – 17 eV have found application in **photovoltaic conversion**. Most of the effort has been placed into Cu(In,Ga)Se$_2$ system, also, CuInS$_2$ is one of the favourites. Using a solid solution of two ternary chalcopyrites, the bandgap of the resulting crystal can be tuned in a large range. For example, the system CuIn$_x$Ga$_{x-1}$Se$_2$ allows bangap engineering from the bandgap values of 1.00 eV (stoichiometric CuInSe$_2$ [6]) to 1.7 eV (stoichiometric CuGaSe$_2$ [7]). The photovoltaic devices with Cu(In,Ga)Se$_2$ absorber material and CdS buffer layer have reached 19.2% efficiency [8].
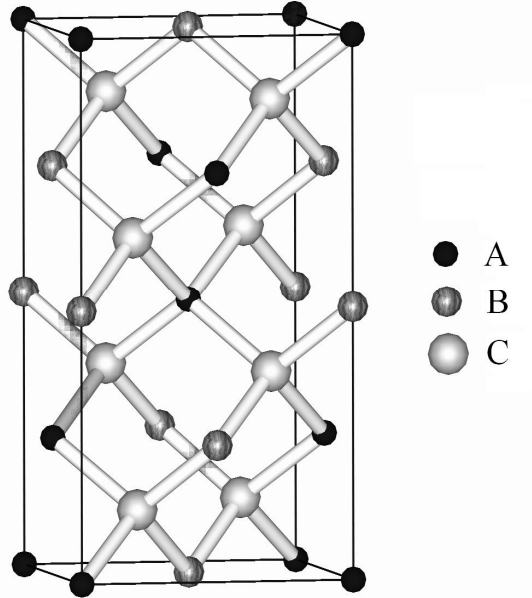

Figure 1. Chalcopyrite crystal lattice. The unit cell has a tetragonal shape. Stoichiometric chalcopyrite structure has a configuration A-B-C$_2$. The first type of chalcopyrites are formed from I-III-VI$_2$ elements and the second from II-IV-V$_2$ elements.

Being a good absorber, chalcopyrite material can, at the same time, be a good emitter as well. Thus, this material class can be used in optoelectronics as electroluminescence emitter. For example, one can get greenish-white electroluminescence from p-type CuGaS$_2$ heterojunction diodes [9].

Figure 1 shows the crystal lattice structure of chalcopyrite semiconductors. The lattice type is a primitive tetragonal. The I-III-VI$_2$ group chalcopyrites are formed from A = (Cu, Ag), B = (Al, Ga, In), and C = (Te, S, Se) elements. The II-IV-V$_2$ group semiconductors are formed from A = (Zn, Cd, Hg), B = (Si, Ge), and C = (P, As, Sb) elements.

3.2   Chalcopyrite tellurides

Chalcopyrite tellurides belong to the group of ternary compounds I-III-Te$_2$. There are six different materials that can be formed:

1) $CuAlTe_2$,
2) $CuGaTe_2$,
3) $CuInTe_2$,
4) $AgAlTe_2$,
5) $AgGaTe_2$,
6) $AgInTe_2$.

Despite their many promising applications, not many papers have been published on chalcopyrite tellurides. Based on the search engines of "ISI Web of Science" [10] and "ScienceDirect" [11] databases, there are only 310 published *Current Contents* papers between 1969 and 2006 that study the properties of these materials. Over the years, the number of published papers has slightly increased, but not much (see Figure 2). Most of the papers (147) have been published on $CuInTe_2$. The reason that this material has received more attention than the others is its application in photovoltaic devices. Other ternary tellurides have enjoyed the attention of 63 ($CuGaTe_2$), 44 ($AgInTe_2$), 33 ($AgGaTe_2$), 20 ($CuAlTe_2$), and 2 ($AgAlTe_2$) papers, respectively, between the years 1980 and 2006. Most of the studies concentrate on optical and electrical properties. The main analytical tools are photoluminescence spectroscopy, Raman spectroscopy, absorption spectroscopy, and X-ray diffraction. Also, few papers study the mechanical properties of these materials. The reason why only two papers have been published on $AgAlTe_2$ is that these nice looking orange-red crystals are very hard to handle. The crystals are brittle and oxidize very rapidly in the air [12].
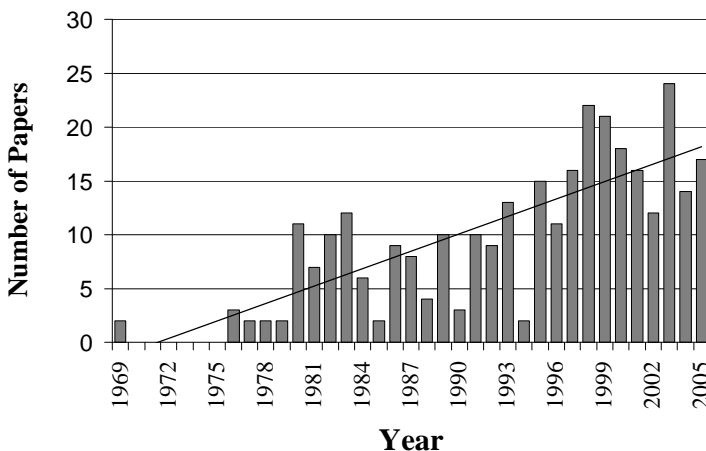

Figure 2. Number of papers published on chalcopyrite tellurides per year. Linear regression shows a steady increase.

Table 1.2. Parameters of chalcopyrite tellurides

	Bandgap energy E_g, (eV) room temp. if not stated otherwise	Conductivity type	Unit cell parameters[13]		Melting point (°C)
			a (Å)	c (Å)	
CuInTe$_2$	0.96[14] 0.98[15][16] 0.945[17] 0.99[18] 1.03[19]	p[28][29]	6.167	12.34	789[31]
CuGaTe$_2$	1.18-1.33[20] 1.21-1.24[21]	p[31]	5.994	11.91	865[31]
CuAlTe$_2$	2.45[22] 2.06[23] 2.35[24]	p[31]	5.964	11.78	
AgInTe$_2$	0.93-0.96[23] 1.12-1.26[25] 0.96[12] 1.04@77 K[12]	n[12][31] p[12][31]	6.406	12.56	672[30] 692[31]
AgGaTe$_2$	1.09[26] 1.1[23] 1.32[27] 1.36@77 K[12]	p[12][31]	6.283	11.94	711-721[26] 715[31]
AgAlTe$_2$	2.35@77 K[12] 2.27@77 K[13]	p[12][31]	6.296	11.83	

Some of the important parameters of chalcopyrite tellurides are listed in Table 1.2. The parameters depend strongly on the stoichiometry of the crystals. In chalcopyrites, **ordered vacancy compounds** can be formed rather easily. In that case, some specific defect is periodically introduced into the crystal lattice, thus, new compounds like I-III$_3$-VI$_5$, I-III$_5$-VI$_8$, etc. are formed. This might also be the reason why the **band gap energies** by different authors vary so much (see Table 1.2). On the one hand, researchers might have to deal with ordered vacancy compounds of I-III-V elements, also, a mixture between the ordered vacancy compound and the stoichiometric crystal lattice is possible. In addition, discrepancies in experimental bandgap values come from different measurement methods used.

Some chalcopyrite materials from the I-III-VI$_2$ group tend to have p-type conductivity, some have n-type conductivity, and the conductivity type of some of the materials can be tuned with doping [32]. Within chalcopyrite tellurides only p-type and tunable materials have been observed, i.e. no chalcopyrite tellurides have been found to have only n-type of conductivity. Cu-based tellurides tend to have only p-type conductivity while the inclusion of Ag shifts the Fermi level towards the conduction band. It is believed that with the substitution of Cu with Ag the probability of I element vacancy formation decreases and the formation of anion vacancies turn out to be energetically favorable. Thus, compound will exhibit n-type conductivity [32].

In the present thesis, four of the six chalcopyrite telluride semiconductors are studied. The main analytical tool is **low-temperature photoluminescence spectroscopy**. The studied compounds are $CuInTe_2$, $CuGaTe_2$, $AgInTe_2$, and $AgGaTe_2$. The reason why Al containing compounds were left out is their deficiency, partially caused by reasons stated above.

3.3 Overview of previously published papers

3.3.1 CuInTe$_2$

The photoluminescence properties of $CuInTe_2$ have been previously reported by two groups. The first group is, **Hideto Miyake** group from Japan, Department of Electrical and Electronic Engineering, Mie University. The second group is led by **Carlos Rincón**, located at Centro de Estudios de Semiconductores, Universidad de Los Andes, Venezuela.

Miyake *et al.* have studied chalcopyrite $CuInTe_2$ structures that were grown by the traveling heater method [33]. The photoluminescence spectra were recorded at liquid nitrogen temperature 77 K. The spectrum consisted of one broad peak centered at 1.02 eV. The authors claim that this peak might originate from conduction band to shallow acceptor transition. The shallow acceptor is probably a Cu vacancy.

More detailed studies were conducted by Rincón *et al*. In [34] the authors study the $CuInTe_2$ photoluminescence spectrum dependency on excitation intensity and in [35] they analyze the dependence on the sample temperature. In both papers, they concentrate on the edge photoluminescence emission. Ref. [34] describes photoluminescence measurements at 4.2 K with various excitation energies from 1.8 W to 0.1 W. The authors found 8 photoluminescence bands which were identified as free-exciton (at 1.053 eV), bound-exciton (at 1.047, 1.044, 1.040, and 1.030 eV), donor-acceptor pair recombination (at 1.022, and 1.017 eV) and donor-to-valence band recombination (at 1.033 eV). The reported values of activation energies for the donor and acceptor levels are $E_{a1} \approx 14$ meV, $E_{a2} \approx 75$ meV, $E_{d1} \approx 25$ meV, and $E_{d2} \approx 58$ meV, respectively. The estimated free exciton binding energy is 6 meV. The authors do not attribute the defect levels to any particular point defect.

Temperature dependent photoluminescence experiments were conducted in [35]. The spectrum was recorded at various temperatures from 10 K to 120 K. As a result, two photoluminescence bands were found. According to the authors' analysis, the origins of the emission bands are ground-state free exciton (at 1.053 eV) and bound exciton (at 1.047 eV) recombinations. The calculations in [35] prove that the binding energy of the free exciton is 6 meV. Also, it is reported that the bound exciton binding energy with acceptor is about 14 meV, which is in good agreement with their previous paper [34]. The authors claim that most probably the acceptor level is caused by Cu_{In} or V_{In} point defects.

A theoretical paper on the ternary compound is published by the same group from Venezuela [36]. This paper reports theoretical activation energy of many

chalcopyrite compounds. The model used is based on the effective-mass theory. As a result, the following activation energies were calculated for acceptors in CuInTe$_2$ 70, 120, 180, 290,400, and 650 meV. For donors the reported values are: 15, 26, 37, 60, 85, and 138 meV.

3.3.2 CuGaTe$_2$

The first photoluminescence spectrum of CuGaTe$_2$ was published by **G.Massé** *et al*. in [37]. The figures in this paper depict the experimental photoluminescence spectra from 77 K to 300 K. The authors distinguish four photoluminescence bands centered approximately at 1.32, 1.34, 1.40, and 1.42 eV. The first band was interpreted as free to bound recombination between conduction band and shallow acceptor. The second and the third bands were identified as free-to-bound transitions that involve Te vacancy. The fourth band was attributed to donor-acceptor pair recombination that also involves Te vacancy.

More detailed studies of the photoluminescence properties of CuGaTe$_2$ have been conducted by **J.Krustok** *et al*. in [38] and [39]. In [38] edge photoluminescence was observed with well resolved bands at 1.431 eV, 1.426 eV, 1.417 eV, and 1.338 eV. The bands had also well resolved phonon replicas. From the analysis of temperature and laser-power dependencies it was concluded that the 1.431 eV band has excitonic origin. This conclusion was also supported by the narrowness of this band. The fitting of the thermal quenching of this band resulted in the activation energy of 8.7 meV. The second band at 1.426 eV had activation energy of 22 meV. The origin and the activation energy involved in the third band remained unsolved. The fourth band indicated two activation energies 14 meV and 65 meV.

The second paper by Krusok *et al.* [39] describes the deep photoluminescence region of CuGaTe$_2$ samples. The deep band observed is centered at 0.95 eV. The band did not shift with laser power variations but showed noticeable shift with temperature variations. Based on these facts it was concluded that the origin of this band is a recombination process that happens near the potential gradient in the crystal's electric field. It was discussed that the gradient in the potential field may occur due to dislocation or a grain boundary. The recombination channel itself opens between the conduction band and the acceptor level. The acceptor level activation energy 200 meV was calculated from a thermal quenching experiment.

Similar bands like Krustok *et al.* reported in [38] and [39] were found by **P.Guha** *et al*. in [40]. They reported of two peaks that were located at 0.8 eV and 1.32 eV at 80 K.

3.3.3 AgInTe$_2$

To our knowledge only one paper has been published on the photoluminescence properties of AgInTe$_2$ [12] long time ago by B.Tell *et al.* in 1974. The paper reports one near-band-gap broad band at about 0.97 eV.

3.3.4 AgGaTe$_2$

Photoluminescence experiments on AgGaTe$_2$ have been mainly conducted by **I.V.Bodnar** *et al*. The measurements were reported in [41, 42, 43]. In [41, 42] two emission regions were described in single crystals grown by the Bridgman technique. The narrow edge emission peak at 1.34-1.35 eV is attributed to the excitonic emission while the deep broad emission band at 0.85-0.87 eV is attributed to the donor-acceptor pair (DAP) recombination. A similar deep band is also reported in [43] by **M.C.Ohmer** *et al.* where the origin of the emission is assigned to native defect states.

3.4 The aim of this work

It can be seen that not many papers have been published on the photoluminescence of chalcopyrite tellurides. Despite good work of many above mentioned authors, many questions have remained unanswered. What is the main radiative recombination process in heavily doped CuInTe$_2$, CuGaTe$_2$, and AgGaTe$_2$ materials? What is it like and what are the origins of the deep emission of CuInTe$_2$ samples? From the literature overview it can be seen that almost nothing is known about photoluminescence properties of AgInTe$_2$.

The aim of this work is to clarify the radiative recombination processes in chalcopyrite tellurides and to answer the stated questions.

4   Experimental

4.1   Photoluminescence measurements

   All the experiments were conducted at the Department of Materials Science, Tallinn University of Technology. A standard photoluminescence measurement setup was used. The photograph of the laboratory equipment can be seen in Figure 3. The schematic view of the setup is depicted in Figure 4.

   The sample is mounted into the closed-cycle helium cryostat that is

Figure 3. Experimental setup of photoluminescence measurements at Tallinn University of Technology.
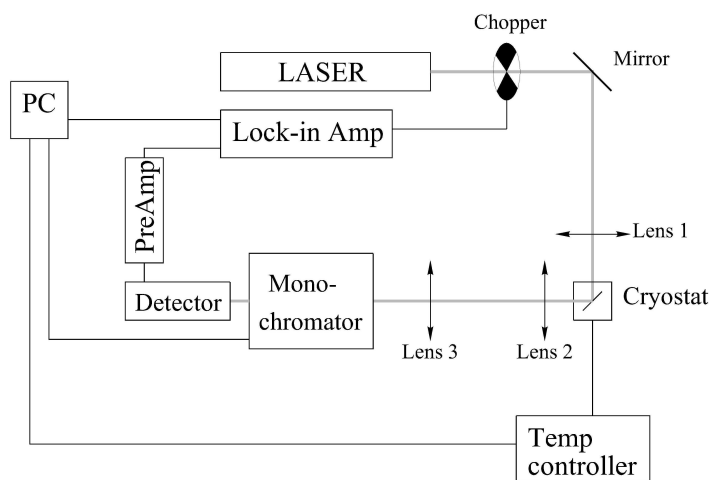

Figure 4. Schematic view of the photoluminescence setup.

connected with a temperature controller. In such a system the temperature can be controlled from 8.4 – 325 K. The cryostat has quartz windows, thus, measurements of infrared emission are possible. Moreover, all the other optical devices, e.g. lenses are made from quartz for the same reason. The sample is mounted inside the cryostat onto a vertical plane surface of the cold head using silicon grease as adhesive material. Silicon grease was chosen because it does not emit a low temperature photoluminescence signal in the infrared region. If it was possible, the photoluminescence signal would always be measured from the freshly cleaved surface.

The sample is optically excited with a laser. During our experiments we used two types of lasers. The first one was He-Cd tube laser with maximum output beam power 45 mW for blue 441.6 nm laser line and 15 mW for ultraviolet 325.0 nm laser line. The choice of the laser lines used could be made by inserting dedicated filter on the output beam path of the laser. The second laser used was a solid state laser with the maximum output power of 60 mW with the wavelength of 675 ± 15 nm. The output power of both of the lasers could be tuned with the set of grey filters that were placed in the filter stage. The output power of the laser beam was calibrated with the laser power meter *Melles Griot 13PEM001*.

The laser beam was focused on the sample with 3-axis movable lens (Lens 1 in Figure 4) with a focal length of 20 cm. In the cases when several samples are placed into the cryostat, the movement of the lens in the perpendicular direction with respect to the laser beam, allows us to choose between the samples. Also, it allows choosing different spots on the sample's surface.

The luminescence signal was collected with Lens 2 that has a focal length of 10 cm. If it is positioned exactly 10 cm from the sample, the sample is in the focus and after the lens, a parallel beam is formed. Next, the parallel beam is focused with Lens 3 into the entrance slit of the monochromator. The focal length of Lens 3 matches exactly the focal length of the monochromator, which is 40 cm.

The model of the monochromator is *Carl Zeiss SPM-2*. It has changeable dispersive element, thus, depending on the required resolution and spectral region, 600 lines per mm grating, 300 lines per mm grating, or prism can be used. The dispersion of the system with gratings ranges from 1.39 to 8.33 nm per 1 mm of the slit width, depending on the grating and grating order. The monochromator is motorized with a self-made system controlled with by a PC.

Monochromatic light that exits the exit slit of the monochromator is detected with a detector. The available detectors were *Hamamatsu* **InGaAs** which we used for the spectral region from 0.6 to 1.7 eV, **PbS** detector that senses from 0.5 to 2.5 eV, and **photomultiplier tubes** *FEU79* and *R632* with spectral sensitivity from 1.5 to 3.5 eV, and 1.2 to 2.7 eV, respectively. The signal from the detectors was first pre-amplified and then detected with a *Stanford Research Systems SR810DSP* **lock-in amplifier**.

4.2 Software

The software that controls the photoluminescence system was written on **TestPoint platform**. TestPoint is a programming environment that is specially designed for laboratory equipment control. The software scans the spectrum that exits the monochromator slit from the desired range, at the same time recording the signal from the lock-in amplifier. Also, the software controls the temperature controller. This allows the measurements of temperature dependence of the photoluminescence spectrum to be left for automatic overnight scanning without human intervention. The measured spectra were fitted with the solver function of **MS Excel** or **Microcal Origin** software.

4.3 Sample preparation

4.3.1 CuInTe$_2$

We studied two types of CuInTe$_2$ samples. Firstly, we studied monocrystalline samples that were made by **Dr. Mike Yakushev** at the **Department of Physics and Applied Physics, University of Strathclyde, Glasgow**. Single crystals of CuInTe$_2$ were grown by the vertical Bridgman technique, which is also used to fabricate CuInSe$_2$ and other chalcopyrite ternary compounds. The pseudo binary phase diagram of CuInTe$_2$ was first reported by Palatnik and Rogacheva [44]. A close to stoichiometric mixture of high purity (99.999%) Cu, In and Te was sealed in vacuum in a thick wall quartz ampoule of 20 mm internal diameter. The mixture was prereacted at about 1000°C for two hours in a rocking furnace and solidified in the horizontal position. Then the ampoule was introduced into the upper (hot) zone of a two-zone vertical furnace. In this position, the prereacted material was melted again and held at 1000°C for six hours. Then the temperature of the higher zone was reduced to 850°C, which is above the melting point $T_m = 789^{\circ}$C [10]. The lower zone temperature was held at 750°C. For solidification, the furnace was slowly moved up, translating the ampoule into the lower zone at a speed of 2 cm a day. After solidification the ampoule was slowly cooled at two rates: 1°C/h from 750°C to 600°C and 5°C/h from 600°C to 20°C.

X-ray diffraction analysis on the grown ingot indicated the presence of the single CuInTe$_2$ chalcopyrite phase. The photoluminescence of the single crystalline samples showed one broad peak in the edge emission region. This implies a large concentration of defects.

Secondly, the **polycrystalline** samples were made by **Dr. Jaan Raudoja** at **Department of Materials Science, Tallinn University of Technology.** The samples were synthesized from elements at 810ºC in fused quartz ampoules. The treatment continued with homogenizing annealing at 665ºC, which is slightly lower than the peritectic temperature in CuInTe$_2$ [3]. The starting Cu/In concentration ratio was 1.03. The final polycrystalline CuInTe$_2$ ingot showed a well-defined chalcopyrite pattern in the XRD scan. The photoluminescence spectrum of those samples showed well-resolved peaks with the phonon

structure. We detected both edge and deep photoluminescence emission. Moreover, the photoluminescence signals were strong enough to record the power and temperature dependences of these spectra.

4.3.2   CuGaTe$_2$

The polycrystalline CuGaTe$_2$ material was synthesized by Dr. Jaan Raudoja at Tallinn University of Technology. The precursor materials had 5N-purity components. The phase equilibrium data was taken from [45]. Cu, Ga and Te were weighted according to the stoichiometric molar ratios 1:1:2. The materials were loaded into the quartz ampoule, evacuated to high vacuum and sealed. The synthesis proceeded at the temperature of 900° C in the muffle furnace for 24 hours. Then the ampoule was cooled slowly (0.3 deg/h) in the region of the crystallization point (895° C to 865° C), followed with the rate of 10 deg/h to the room temperature. From the analysis of x-ray powder diffraction patterns, the single-phase nature and the chalcopyrite structure of the material were confirmed. The samples showed a well-resolved edge emission region with many peaks and also a deep photoluminescence region with two broad peaks.

4.3.3   AgInTe$_2$

The AgInTe$_2$ samples were grown by Dr. Jaan Raudoja at Tallinn University of Technology. The polycrystalline material was synthesized from high purity (5N) elements. The components were weighed out according to the stoichiometric ratio and loaded into a quartz ampoule. The ampoule with precursor materials was degassed and evacuated up to 0.0133 Pa. Then the ampoule was sealed. The synthesis of the material started at 710°C for 24 hours. Then the temperature of the furnace was slowly reduced with the rate of 1°C/8h to the crystallization point of the AgInTe$_2$ (692°C [10]). After crystallization, the material was cooled down to the room temperature with the rate of 10°C/h. The photoluminescence spectrum of AgInTe$_2$ showed well-resolved emission spectrum with excitonic peaks and phonon replicas. Also, a deep region of photoluminescence was detected. The XRD analysis of the synthesized samples confirmed the expected chalcopyrite AgInTe$_2$ structure (see Figure 5a). No other phases were detected.
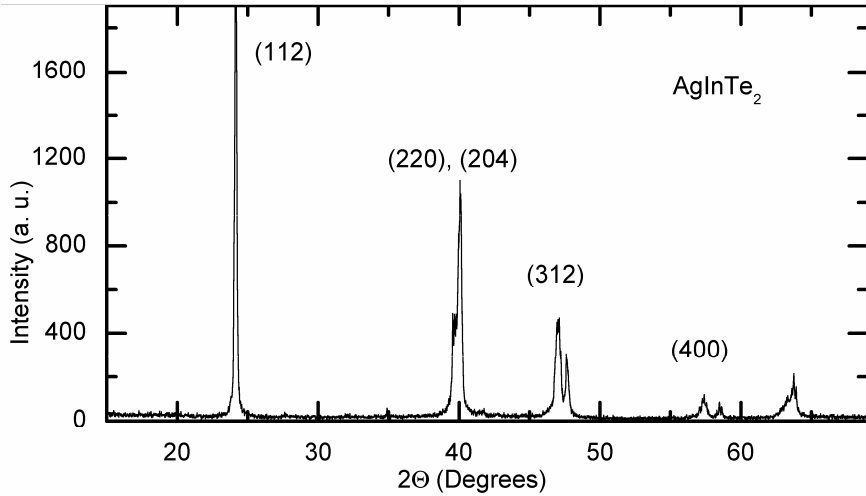
Figure 5a. Measured X-ray diffraction spectrum of the AgInTe$_2$ sample.

4.3.4 AgGaTe$_2$

The polycrystalline AgGaTe$_2$ material was synthesized by Dr. Jaan Raudoja at Tallinn University of Technology from 5N-purity components. The phase equilibrium data was taken from [31]. The elements Ag, Ga, Te were weighted according to the stoichiometric molar ratios of 1:1:2. The materials were inserted into the quartz ampoule, which was then put into high vacuum and sealed. The synthesis was carried out in the muffle furnace. In order to obtain a homogenous material, the ampoule was first held at 750 ℃ for 24 hours. Then

Figure 6. XRD spectrum of polycrystalline AgGaTe$_2$ samples.

21

slow cooling (0.5 ℃/h) was carried out in the region of the crystallization point (730 ℃ to 710 ℃). Final cooling followed at the rate of 5 ℃/h until the room temperature was achieved. The XRD measurements of the samples showed pure chalcopyrite $AgGaTe_2$ phase, see Figure 6.

5 Theory

5.1 Photoluminescence

Photoluminescence is the optical radiation emitted by a physical system resulting from excitation to a nonequilibrium state by irradiation with light [55]. The photoluminescence process can be divided into four sequentially
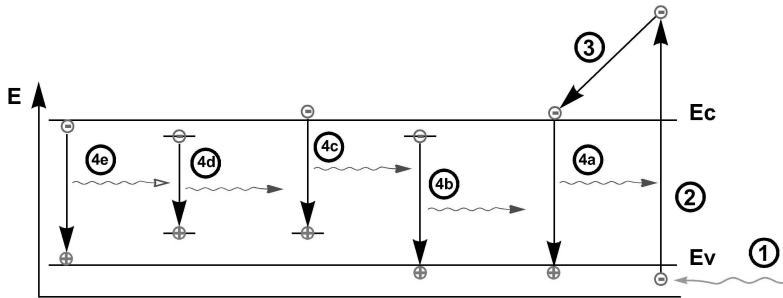

Figure 7. Basics of photoluminescence. After absorption, an electron is energized to the conduction band where it rapidly reaches a thermal equilibrium with the lattice (process 3). The energy of the exciting photon (1) is always higher than the energies of the emitted photons (4a, 4b, 4c, 4d, and 4e).

happening events. In the first event (no.1 in Figure 7), light that has larger photon energy than the bandgap of the semiconductor material under study, is absorbed in the crystal. As a result, an electron is excited from the valence band to the conduction band (event no. 2). A hot free electron and a free hole are created. During event no. 3 the excess energy of the electron is given to the crystal lattice and the electron relaxes to the bottom of the conduction band. This process is usually rather fast, thus, it is not very often that hot electron recombination is detected. It happens only when the sample is degenerate and the Fermi level is in the conduction band. Event no. 4 is the recombination of the electron and a hole. As a result, a photon is emitted. The emitted photon energy is always smaller than the energy of the exciting photon. In the photoluminescence spectrum, several recombination channels may be detected. The most common radiative recombination channels are:

1) Band-to-band recombination (no. 4a),
2) Donor-to-band recombination (no. 4b),
3) Band-to-acceptor recombination (no. 4c),
4) Donor-acceptor pair recombination (no. 4d),
5) Excitonic emission (no. 4e).

Merely the position of the photoluminescence peak does not indicate what the origin of the radiation is, but Figure 7 gives an idea where they might be positioned on the energy scale relative to the excitation source.

The excited volume of the sample depends on the penetration depth of the exciting light; accordingly, if the diffusion length of the incident light is longer, the bigger volume is excited. In turn, diffusion length depends on the absorption coefficient of the material. On the other hand, the photon emission from the recombination is a subject to self-absorption and will not propagate very far. In sum, it is expected that the photoluminescence signal comes from the very shallow layers of the excited crystal.

There are three positive factors of photoluminescence as a material research tool. The first is its sensitivity; photoluminescence spectrum is very sensitive to small changes in the crystal structure and doping quality and quantity. The second factor is its simplicity regarding sample preparation. Samples do not need any specific preparation in terms of polishing, etc. Also, materials from bulk crystals to thin films can be studied. The third advantage is the simplicity of the experimental setup.

The only disadvantage is that the information gained from the photoluminescence experiment requires very often detailed and complicated analysis. The models that describe the physical phenomenon behind the detectable photon emission are quite complex and sometimes it is difficult to assign one or another photoluminescence feature to a specific physical origin. For this reason, usually many spectra of the same sample are recorded with various temperatures and excitation energy conditions to intensify the features of the physical phenomena happening inside the sample.

5.2 Heavily doped semiconductors

Heavily doped semiconductors are those in which the average distance between impurities is less than the Bohr radius of an impurity state [46].

In other words, if the condition $N \cdot a_b^3 > 1$ (where N is **defect concentration** and a_b is **Bohr radius** of the defect state) is satisfied, we have to deal with the theory of heavily doped semiconductors. In that case the kinetic energy of an electron localized in a region of size $N^{-1/3}$ is higher than the potential energy of the Coulomb attraction by a donor. The shallow impurity levels in that case are smeared out in the energy scale and overlap with band states. For all of these reasons, the states of the charge carriers are not governed by single impurity, but rather by the field created by all the impurities and carriers in a given semiconductor sample. This many-body interaction broadens the energy levels of the deep impurity state. In sum, the so-called impurity bands and **density-of-states tails** in the bandgap are formed (see Figure 8.). The **density of states function** $\rho(E)$ does not vanish at the unperturbed edges of forbidden band. The charge carriers that do not have enough energy to travel freely along the crystal feel the perturbation areas as potential wells.
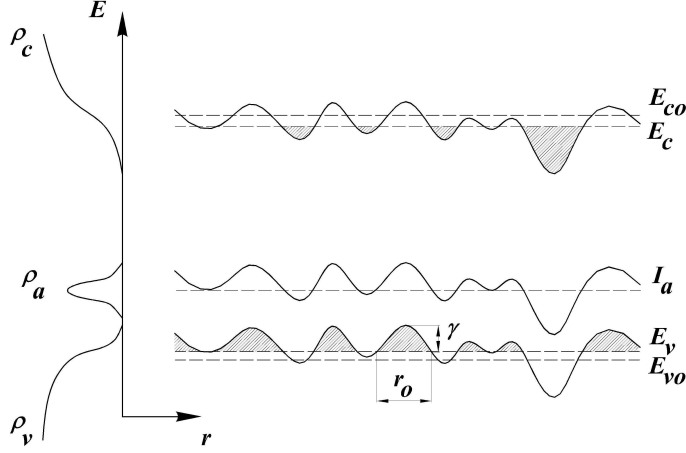
Figure 8. Band diagram of heavily doped semiconductors. Because of heavy doping, band edges start to fluctuate in space. E_{co} and E_{vo} are the forbidden zone edges without heavy doping. E_c and E_v are the levels where electrons and holes, respectively, can be considered as free particles. As a result, it seems that the bandgap has decreased. r_0 and γ mark the average potential well width and depth. ρ_c, ρ_a, and ρ_v are the density of states functions of the conduction band, defect state and valence band, respectively.

Another feature of heavily doped samples is that the **Thomas-Fermi screening radius** r_0 is smaller than the Bohr radius a_e [46]:

$$r_0 = \left(\frac{\pi}{3}\right)^{1/6} \left(\frac{a_e}{4n^{1/3}}\right)^{1/2} \approx \frac{1}{2} a_e \left(na_e^3\right)^{-1/6} < a_e, \tag{1}$$

where n is the concentration of free electrons. The characteristic size of a potential well is equal to the screening radius r_0 and its **root-mean-square depth** is [36]

$$\gamma = \sqrt{2\pi} \frac{e^2}{\varepsilon r_0} \sqrt{Nr_0^3} \ . \tag{2}$$

Heavy doping does not necessarily mean doping with impurity atoms. The conditions of heavy doping may also originate from the high concentration of native defects, i.e. interstitials, vacancies, etc. The chalcopyrite class of materials is known to have large concentrations of native defects, thus, it is expected that from the photoluminescence spectra of chalcopyrite tellurides, we observe many phenomena that originate from the condition of heavy doping.

5.3 Photoluminescence of heavily doped semiconductors

Because of the special energy spectrum of charged particles in heavily doped semiconductors, the radiative recombination processes in these materials are rather complicated.

In the following discussion it is assumed that the **effective mass** of the conduction band electrons is much lower than that of the valence band holes $m_e^* \ll m_h^*$. Indeed, according to Ref. [36], the effective masses of holes in I-III-VI$_2$ materials are 3.1 – 8.1 times grater than the effective masses of electrons. Based on this assumption, it is possible to predict what kind of recombination channels prevail in samples with different types of doping.

In the case of an n-type heavily doped semiconductor, the conduction band tail has virtually no effect on the photoluminescence spectrum. Because of the low effective mass of electrons, it is impossible to confine them in rather small potential wells. On the other hand, heavy holes are easy to trap in the potential wells of the valence zone; accordingly, new features appear from the localization of holes. In sum, three types of recombination channels govern the photoluminescence spectrum of heavily doped n-type semiconductors (see Figure 9). The first is **band-to-band recombination (BB)**, where a free electron recombines with a free hole. The second is **band-to-tail recombination (BT)**, when a free electron recombines with a hole that is localized in the conduction band tail. The third is **band-to-impurity recombination (BI)**, where a free electron recombines with a hole that is localized on a deep acceptor state.

In the case of p-type heavily doped semiconductors, the Fermi level is closer to the valence band and the probability of electron localization in a potential well of the conduction band is higher. Accordingly, in addition to the BB, BT,
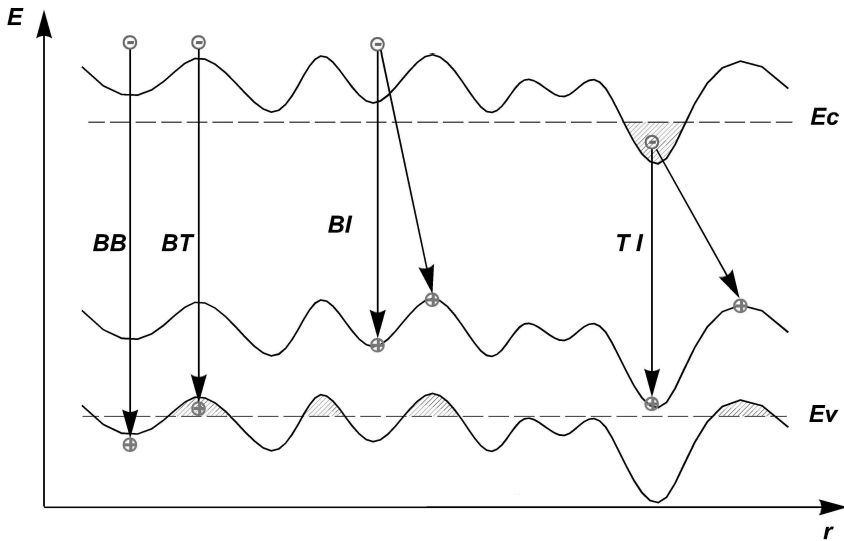

Figure 9. Radiative recombination channels in heavily doped semiconductors. In the case of small electron effective mass and high level of Fermi energy, BB, BT, and BI recombinations dominate. In the case of high electron effective mass and low level of Fermi energy, TI recombination becomes more probable. E_c and E_v are the levels from where the electrons and holes, respectively, can be considered as free.

and BI recombination bands, **tail-to-impurity (TI)** and **tail-to-tail (TT)** bands emerge. In Chapter 4 BB, BT, BI, and TI bands are discussed in detail. Some theoretical discussions are covered in the results section, because it is more convenient to discuss the theory of the photoluminescence bands side-by-side with real experimental examples. Our selection is based on the bands that were identified in the photoluminescence spectra of chalcopyrite telluride samples. Specifically, we have observed BB and BT recombination in $AgGaTe_2$, BI recombination in $AgGaTe_2$ and $CuInTe_2$, and TI recombination in $CuGaTe_2$ crystals.

6 Results

6.1 CuInTe₂

6.1.1 Single crystalline samples of CuInTe₂

Let us first discuss the results of the photoluminescence experiment on single crystalline CuInTe₂ samples, which were grown in University of Strathclyde, Glasgow. The growth procedure was described in Chapter 2. Those samples showed rather strong evidence of heavy doping. According to our analysis, the spectra comprised BI recombination. Thus, let us first discuss some principles of the BI band in heavily doped semiconductors.

The BI – band can be observed if $\gamma_h < I_a$, where γ_h is the mean-square fluctuation of the potential energy of a hole and I_a is the ionization energy of the acceptor state (Figure 10). The theoretical photoluminescence spectrum of this band is defined by the following expression [46]:

$$I(hv) = hv \iint W(E_e, E_h)\rho_c(E_e)f_e(E_e)\rho_a(E_h)q_a(E_h)\delta(E_e - E_h - hv)dE_e dE_h, \quad (3)$$
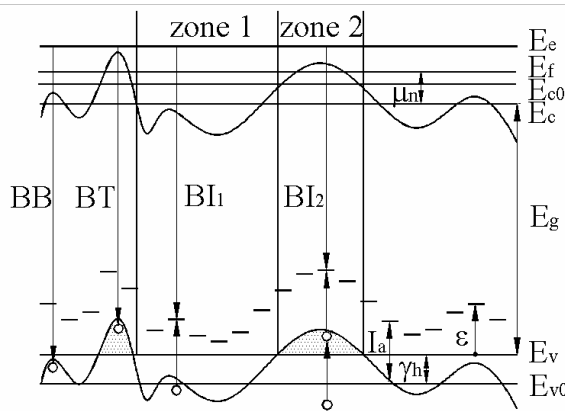

Figure 10. Zone diagram of heavily doped semiconductors according to the theory of potential fluctuation. Holes that recombine through zone 1 are free, and holes through zone 2 are localized. Because of potential fluctuations the ideal upper and lower bandgap edges transform, $E_{c0} \rightarrow E_c$, and $E_{v0} \rightarrow E_v$, respectively. Accordingly, the energy gap of heavily doped semiconductors is somewhat smaller than it would be in the case of a perfect crystal. The acceptor level I_a is "smeared" in the energy scale, therefore, we have to deal with the distribution of the acceptor states rather than a single acceptor level. BI, BB and BT denote band-to-impurity, band-to-band and band-to-tail recombination, respectively.

where $W(E_e, E_h)$ is the recombination probability of a free electron and a localized hole with energies E_e and E_h, respectively, ρ_c is the electron density of states in the conduction band, f_e is the Fermi function, ρ_a is the hole density of states, and q_a is the filling probability of the hole states. As compared to other quantities, W depends very weakly on the electron and hole energies [46], thus it will be treated as a constant.

According to the hole capture kinetics, two recombination neighborhoods can be distinguished. They generate two types of transitions (BI$_1$ and BI$_2$), respectively. The first involves the holes whose energy level is above $E_v = E_{v0} - \gamma_h$, from which they can be considered as free. The filling probability of the impurity states in this zone is as follows [46]:

$$q_a^{BI_1} = \frac{N_0}{N_a} = \frac{p(\varepsilon)}{p(\varepsilon) + \Theta n + N_V \exp(-I_a/kT)} =$$
$$= \frac{p}{p + \Theta n \exp[(I_a - \varepsilon)/kT] + N_V \exp(-\varepsilon/kT)}, \tag{5}$$

where N_0 is the concentration of neutral acceptors, N_a is the total concentration of acceptors, $p(\varepsilon) = p \cdot \exp[(\varepsilon - I_a)/kT]$ is the Boltzmann distribution of free holes, p is the initial hole concentration, ε is the independent energy variable that has the origin at E_v, $\Theta = W_n/W_p$ is the ratio of electron and hole capture probabilities, n is electron concentration, and N_v is the effective number of valence band states.

The capture of the hole by the impurity state in the second zone is a cascade process in which a free hole is localized on the energy tail and then captured by a neutral acceptor. The capture probability in this process is [46]

$$q_a^{BI_2} = \frac{p}{p + \Theta n + N_V \exp(-\varepsilon/kT)}. \tag{6}$$

Reference [60] states that in the case of heavily doped semiconductors, the hole density of states has its maximum at the acceptor's activation energy and has a Gaussian shape: $\rho_a(E_h) = (N_a/\sqrt{2\pi}\gamma)\exp[-(E_h - E_v^0 - I_a)/2\gamma^2]$. According to the free electron model, the electron density of states is $\rho_c(E_e) = (1/2\pi^2)(2m_e^*/\hbar)^{3/2}\sqrt{E_e - E_c}$, where E_c is the energy from which electrons can be considered as free.

Taking into account that the BI-band is the sum of BI$_1$- and BI$_2$–band, we substitute all distribution functions into Eq. (3) and obtain an expression for the theoretical photoluminescence spectrum of the BI-band that can be used for numerical simulations:

$$I(h\nu) \propto h\nu \int_{E_g - h\nu}^{+\infty} \frac{\sqrt{h\nu - E_g + \varepsilon}\,\exp\left(-\dfrac{(\gamma_h - I_a + \varepsilon)^2}{2\gamma^2}\right)}{\left(1 + \exp\left(\dfrac{h\nu - \mu_n - E_g + \varepsilon}{kT}\right)\right)\left(p + \Theta n \eta(\varepsilon) + N_V \exp(-\varepsilon/kT)\right)} d\varepsilon, \tag{7}$$

where $\eta(\varepsilon) = \begin{cases} 1, \text{if } \varepsilon > I_a \\ \exp((I_a - \varepsilon)/kT), \text{if } \varepsilon < I_a \end{cases}$ and $\mu_n = E_f - E_c$ is the difference between
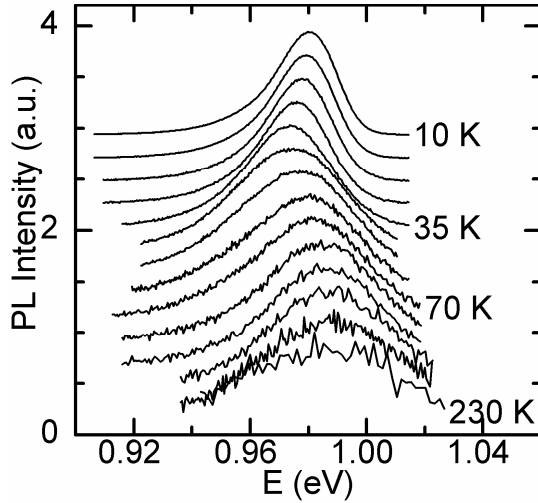
the Fermi level and E_c.

Figure 11. Normalized photoluminescence spectra of CuInTe$_2$ sample measured at different temperatures.
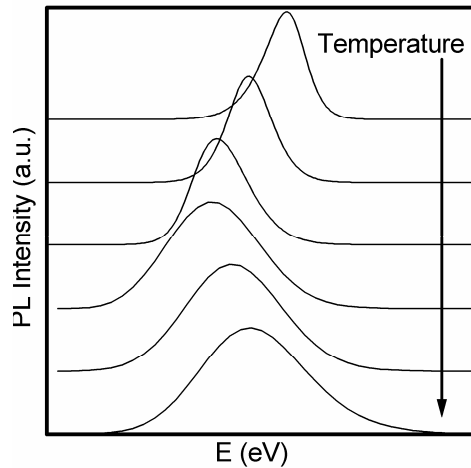

Figure 12. Calculated photoluminescence spectra at various temperatures using Eq. (7). Compared to experimental results (Figure 11), the simulated spectra have the same kind of asymmetric shape. Also, it features the characteristic shift along the energy scale and broadening as it was observed in our experiments.

A typical shape of the photoluminescence spectrum in heavily doped $CuInTe_2$ is asymmetric. It has an exponential slope on the low-energy side and a steeper Gaussian incline on the high-energy side (Figure 11). At low temperature (10 K), its maximum is located at 0.98 eV.

The temperature dependence of the band possesses an interesting quality (Figures 11 and 13). At low temperatures, the peak position energy of the spectrum decreases with increasing temperature, at some temperature T^*, the photoluminescence peak shifts towards higher energy again until it reaches a saturation level. The measured photoluminescence spectra were fitted and compared with computer simulations, which proved that Eq. (7) indicates the same behavior (Figures 12 and 14). The depth of the valley and its position depend on the carriers' concentrations, i.e. on the excitation power. Smaller carrier concentrations correspond to steeper inclines.

Such behavior of hv_{max} can be explained as follows: the transition BI_2 has a maximum probability at temperature T^* after which the thermal activation process starts to dominate and thermalize localized holes into zone 1 (see Figure 10). Accordingly, the maximum of photoluminescence band shifts towards higher energies. The saturation takes place when all localized holes become thermalized. The BI_2 radiation vanishes and the whole recombination goes through BI_1.

A comparison of Figures 11 and 12 shows that the dependence of the measured photoluminescence spectra on the sample temperature is in good conformity with Eq. (7). They both indicate the same type of shift and change in the half-width of the spectra, which widens with the increasing temperature.
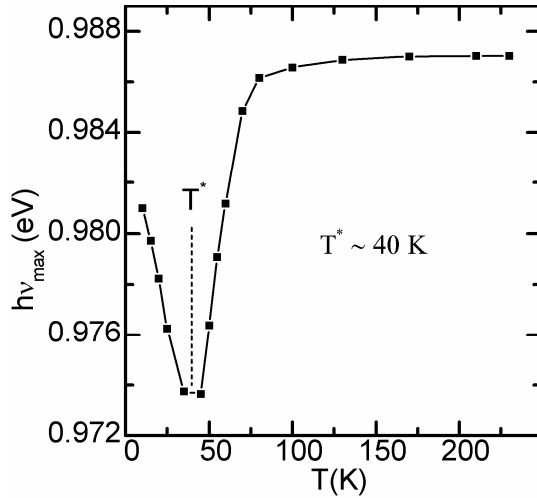
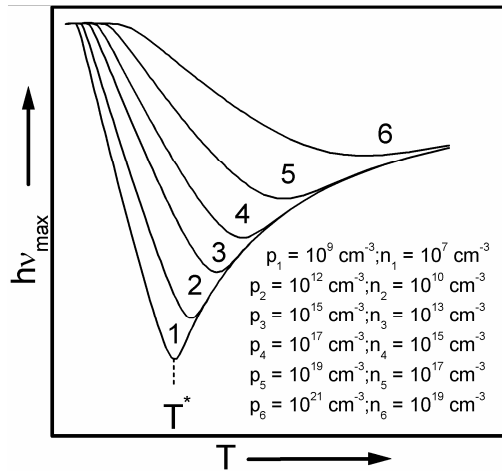**Figure 13**. The shift of CuInTe$_2$ photoluminescence peak position versus temperature.

Figure 14. The dependence of the BI-band peak position on temperature, resulting from computer simulations of Eq. (7). Larger curve numbers correspond to higher carrier densities. The position of T^* is also very sensitive to parameter γ, which characterizes the amplitude of potential fluctuations. If the carrier concentrations are fixed, T^* shifts towards higher temperatures with a higher value of γ. This is coherent with the theory, because in the case of deeper energy tails the holes become more difficult to thermalize.

The theory of heavily doped semiconductors [46] and our simulations prove that at low temperatures the BI-band's maximum is located at $hv_{max} = E_g - I_a$. Whereas the energy gap at 10 K in CuInTe$_2$ is in the range E_g=1.06-1.02 eV [18] and the maximum of our spectrum at 10 K is approximately 0.98 eV, I_a must lie between 40 and 80 meV. According to [36], where the defect levels were calculated theoretically, it can be attributed to the single acceptor level I_a=70 meV, whose possible origins are copper vacancy V_{Cu} or antisite point defects Te_{In} and Cu_{Te}. Though, it is believed that the former has much higher formation probability, the antisite defects must not be totally disregarded.

To endorse the idea of recombination through the acceptor level, the photoluminescence band with a similar activation energy appeared also in not so highly defective CuInTe$_2$ crystal [47], where the phonon structure of the photoluminescence spectra was detected.

The acceptor's activation energy I_a could not be calculated from the traditional Arrhenius plot because in the case of potential fluctuations, the relation Ln(I) versus 1000/T generates no straight line at high temperatures. Indeed, because of potential fluctuations we do not have a single acceptor level but the distribution of the acceptor states around I_a.

The shape of the measured photoluminescence spectra remained unchanged in regard to various excitation powers (Figure 15). Also, no shifts along the energy scale were observed. It means that the shape of the BI-band does not depend on the carrier densities. This implies that the filling probability of the acceptor states is close to uniformity. Again, our computer simulations of Eq. (7) confirmed that the photoluminescence spectra do not depend on the excitation power.
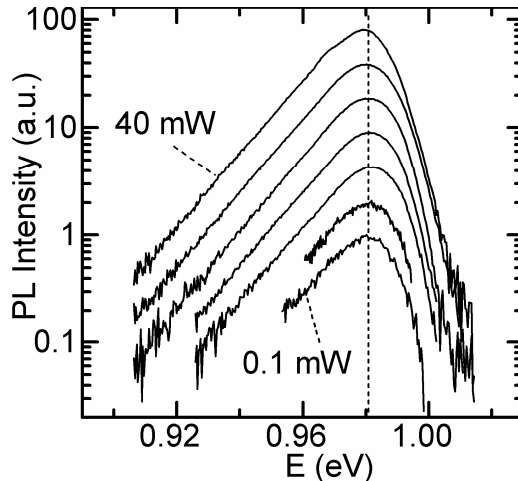

Figure 15. Normalized photoluminescence spectra of single crystalline CuInTe$_2$ sample measured at different laser excitation power.
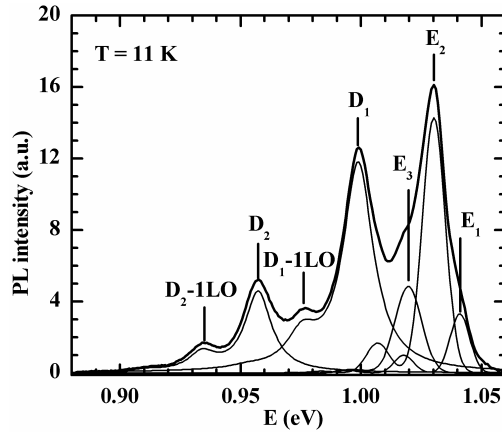
Figure 16. Photoluminescence spectra of polycrystalline CuInTe$_2$ at 11 K. Measured photoluminescence spectra were fitted using five different peaks and their phonon replicas.

The photoluminescence spectra of heavily doped semiconductors are distinctive because of their characteristic asymmetric shape. This distinguishes them from other recombination models. However, the shape of the BT-band is similar to the shape of the BI-band. Thus, it should be carefully considered before attributing the emission to one or the other. While working with other CuInTe$_2$ samples, we have seen both bands on the same spectra. The BI-band appeared exactly in the same position (0.98 eV) and the BT-band had its maximum at about 1.01-1.02 eV.

6.1.2 Polycrystalline samples of CuInTe$_2$

The polycrystalline samples were made in the Department of Materials Science, Tallinn University of Technology. The growth procedure is described in Chapter 2. It is surprising that from the comparison of photoluminescence spectra of monocrystalline and polycrystalline samples, the latter ones indicated lower concentration of native defects, i.e. the photoluminescence spectrum of polycrystalline samples showed excitonic emission and well-resolved phonon structure.

The experimental photoluminescence spectrum of CuInTe$_2$ sample at 11 K is presented in Figure 16. We distinguished five different photoluminescence bands – three near the band-edge bands (E$_1$, E$_2$, and E$_3$) and two deep bands (D$_1$, and D$_2$) with their phonon replicas. We found that the replicas appear in accordance with LO-phonon energy $\hbar\omega_{LO} = 23.2$ meV. The corresponding peak positions and the possible band origins are presented in Table 4.1. The results

were compared with theoretical calculations of defect levels in CuInTe$_2$ [36], where the model of effective mass theory was applied.

We found that three types of recombination mechanisms governed our bands: excitonic, donor to valence band, and conduction band to acceptor emission. It is known that shallow levels, because of the broad amplitude of their wavefunction, tend to form donor-acceptor pairs (DAP). Nevertheless, we can not attribute DAP emission to near-band-edge emission in CuInTe$_2$, because of the overlapping of edge emission bands it was difficult to identify their behavior regarding to excitation power and temperature changes.

The activation energies of relevant defect levels in Table 4.1 were calculated using the expression

$$E_a = E_g - h\nu_{max} , \qquad\qquad (8)$$

where $h\nu_{max}$ is the band's peak position and E_g is bandgap energy. In CuInTe$_2$ E_g is between 1.02 and 1.06 eV [18]. In our calculations we used the value $E_g = 1.06$ eV, which is reasonable, because we observe luminescence intensity up to 1.06 eV.

Edge emission can also be analyzed using the relation $I \sim L^k$ [48, 49], where I is the intensity of the photoluminescence band, L is excitation power, and as a rule k is the factor that is >1 for excitons and ≤1 for non-excitons. Our fitting proved that for E$_1$ k>1, accordingly, it is highly probable that band E$_1$ at $h\nu_{max} = 1.041$ eV has excitonic origin. Allegedly, it is not the consequence of emission by one exciton but rather a sum of several excitonic radiations. Moreover, Refs. [34, 35] report excitonic emission in the same region.

Band E$_2$ at $h\nu_{max} = 1.030$ eV, is not excitonic, because the factor $k < 1$ for this band. Its activation energy according to Eq. (8) is 30 meV, which is in good coherence with the theoretical activation energy of the donor level at 26 meV [36]. Its possible physical origin is telluride vacancy $V_{Te}^{\bullet}$ or antisite defect $In_{Cu}^{\bullet}$ [36].
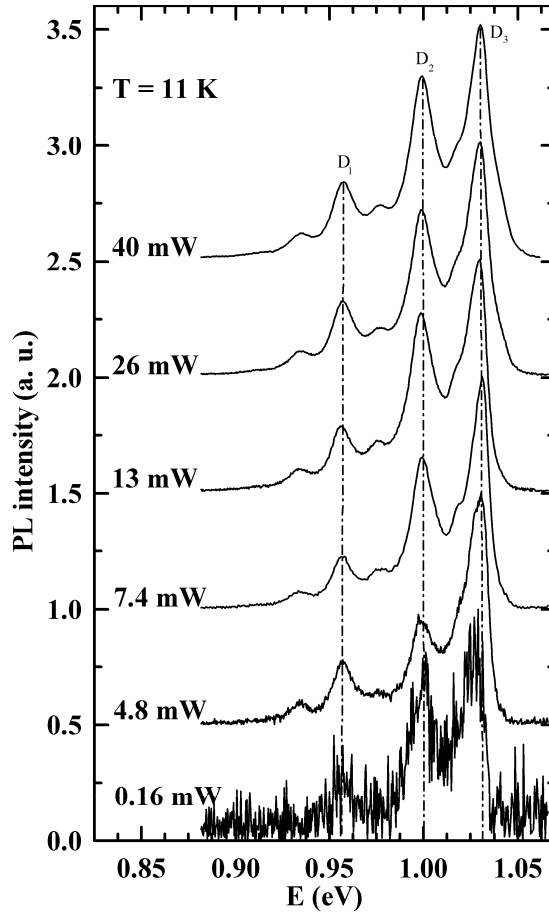
Figure 17.Dependence of normalized polycrystalline CuInTe$_2$ photoluminescence spectrum on laser excitation power. It is evident that peaks D$_1$ and D$_2$ do not shift with altering excitation power, thus, they do not originate from donor-acceptor pairs.

Table 4.1 Experimental values of photoluminescence band positions compared with theoretical calculations. Activation energies were calculated with $E_g = 1.06$ eV.

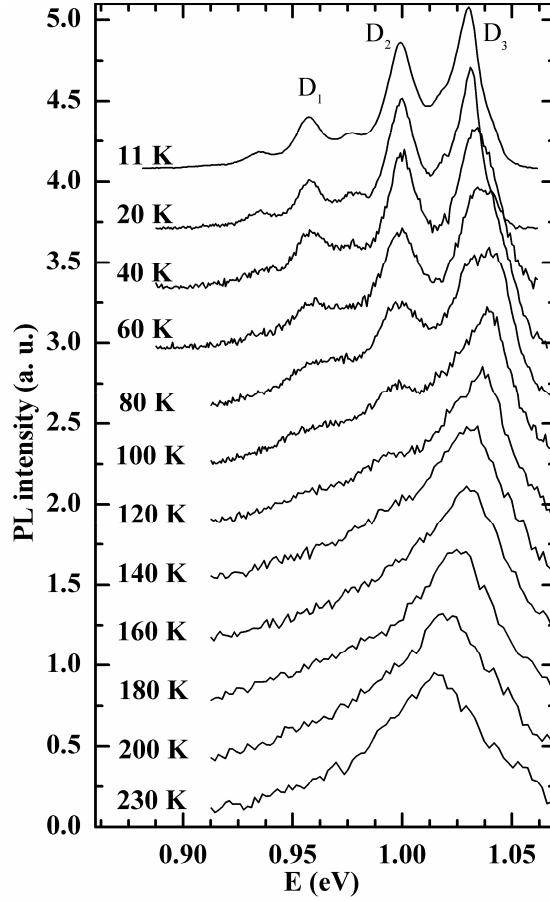| PL band	hv_{max} (eV)	E_a (meV)		Possible origins [36]
		Experimental	Theoretical [36]	
E1	1.041			Excitons
E2	1.030	30	26	$V_{Te}^{\bullet}$, $In_{Cu}^{\bullet}$
E3	1.019	41	37	$In_i^{\bullet}$
D1	0.999	61	70	V_{Cu}' , Te_{In}' , Cu_{Te}'
D2	0.957	103	120	Te_i' , Cu_{In}'

Figure 18. Dependence of normalized CuInTe2
photoluminescence spectrum on sample temperature.

The exact position of band E_3 was not easy to determine, because it is located between two more intensive bands E_2 and D_1. However, the fitting showed that for E_3 $hv_{max} = 1.019$ eV that corresponds to $E_a = 41$ meV. The closest defect level for this is the donor level at 37 meV that is caused by interstitial defect $In_i^{\bullet}$.

The deep bands D_1 and D_2 are most probably radiative emissions between conduction band and an acceptor level. They can not be DAPs because altering the laser power did not generate any j-shift of these bands (see Figure 17). The peak D_1 is located at 0.999 meV and is close to the theoretical acceptor state at 70 meV. We observed the same photoluminescence band in heavily doped CuInTe$_2$ crystal [50]. According to Ref.[36], this band can be caused by copper vacancy V'_{Cu} or antisite point defects Te'_{In} or Cu'_{Te}. The position of peak D_2 ($E_a = 103$ meV) is close to the theoretical deep acceptor level that is situated at 120 meV [36]. Most likely, interstitial Te'_i or antisite defect Cu'_{In} causes this

level. Previously, we observed a deep band with similar properties in the photoluminescence spectrum of CuGaTe$_2$ [38]. Indeed, the Huang-Rhys factor of D$_2$ band is $S \approx 0.22$ while for the deep band in CuGaTe$_2$ it was 0.29.

The temperature dependence of the photoluminescence spectrum of CuInTe$_2$ is presented in Figure 18. In the edge region, excitonic peak starts to dominate if temperature rises, i.e. bands E$_2$ and E$_3$ fade much faster than excitonic E$_1$. The red shift of the edge region can be attributed to the decrease of the bandgap with increasing temperature. Deep bands D$_1$ and D$_2$ can be observed up to 160 K.

6.2 Photoluminescence of polycrystalline AgGaTe$_2$

The polycrystalline samples were synthesized in the Department of Materials Science, Tallinn University of Technology. The growth procedure was described in Chapter 2. The samples showed photoluminescence spectrum that is very characteristic of the heavily doped semiconductors. We observed BB, BT, and BI photoluminescence bands. The classical transition of BT-band to BB-band at higher temperatures was noticeable.

The laser power dependence of the edge emission is shown in Figure 19. In the logarithmic scale, three emission bands can be clearly distinguished. They are located at 1.337 eV (BB), 1.317 eV (BT), and 1.287 eV (BI). The band with the highest intensity (BT band) is visually asymmetric and has a steeper incline on the high energy side. That phenomenon is not common to ordinary band-to-band transition in perfect crystals, where the tilt of the peak should be to the opposite side. Because of strong asymmetry, it is neither common to excitonic nor shallow impurity emission. It should be noted that peak positions found in our samples have lower energy than these measured in single crystals [41, 42]. In single crystals the free exciton (FE) peak at 10 K had a maximum at 1.352 eV and the bound exciton peak was found at 1.338 eV [42]. These facts and the shift of the BT band toward higher energy with increasing laser power (see Figure 19) suggest that the model of heavily doped semiconductors should be applied for our polycrystalline samples.
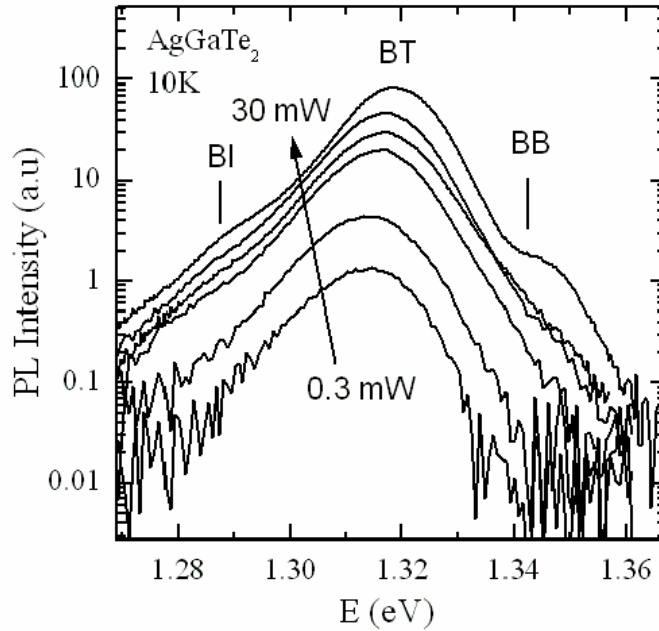
Figure 19. Laser power dependence of the edge photoluminescence emission of AgGaTe$_2$ sample. Three bands are positioned as follows: band-to-impurity (BI) (1.287 eV), band-to-tail (BT) (1.317 eV), and band-to-band (BB) (1.337 eV). The asymmetric shape and the j-shift of the BT band are easily seen.

The temperature dependence of the edge emission spectrum in Figure 20 justifies the assumption of heavy doping. At low temperatures, the BT-band at 1.317 eV prevails and at higher temperatures, the BB-band at 1.337 eV starts to dominate. As the temperature rises, more and more holes that are localized in the valence band tail are thermally liberated. Therefore, the emission transforms from the BT- to the BB-band. The same behavior was observed in CuInGaSe$_2$ [51] and CuGaSe$_2$ [52].

The blue shift of the BT-band with the increasing excitation power (j-shift) (see Figure 19) can be explained by the filling probability of the hole states in the valence band tail. As the excitation power increases, the filling probability of the "shallow states" in the valence band tail also increases and the filling probability of the "deeper states" decreases. Accordingly, the states closer to the unperturbed band edge will be preferentially occupied by holes. Thus, the peak position of the BT-band shifts towards higher energies.
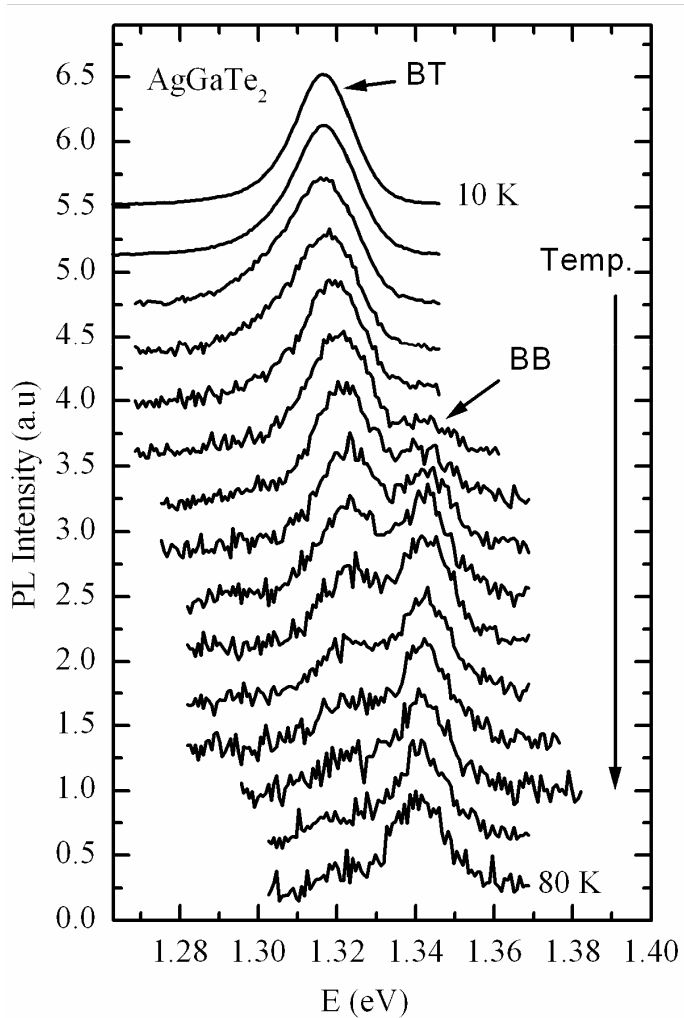
Figure 20. Normalized photoluminescence spectra of the edge emission bands of AgGaTe$_2$ at various temperatures. At low temperatures the band-to-tail emission band prevails. As the temperature rises, the band-to-band recombination starts to dominate.

We observed another asymmetric band at 1.287 eV. This band can be attributed to the band-to-impurity recombination (BI-band). The BI recombination occurs between free electrons, and the holes that are localized at the defect states with the distribution function that does not overlap with the zones. The intensity of the BI-band was not sufficient to obtain the activation energy directly from thermal quenching. However, assuming that the bandgap of AgGaTe$_2$ at 8 K is 1.358 eV [42] and because AgGaTe$_2$ tends to have p-type conductivity, we suggest that the BI-band originates from the conduction band to the shallow acceptor recombination and thus the acceptor's activation energy
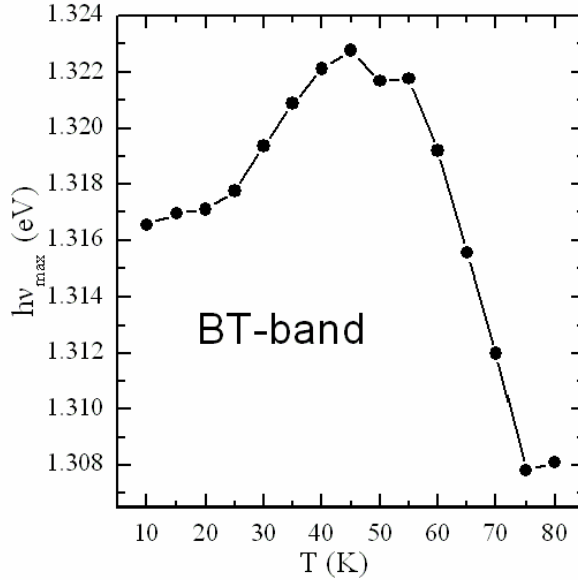
Figure 21. Temperature dependence of the band-to-tail photoluminescence band of AgGaTe$_2$. The shift of edge emission bands is mainly caused by the temperature dependence of the bandgap energy.

can be found by subtracting the BI-band peak position energy from the AgGaTe$_2$ bandgap energy. By doing this we obtain the value of 70 meV.

Figure 21 shows the shift of the BT-band's peak position according to the sample temperature. At low temperatures, the peak shifts towards higher energies with the increasing temperature. This tendency continues to some characteristic temperature where the peak position has its maximum value (1.323 eV at 45 K). After that, the peak starts to shift towards lower energies. A similar behavior was observed in [41, 42]. Because the BT-band position is strongly influenced by the bandgap energy, the shift can be explained by the characteristic bandgap energy temperature dependence of AgGaTe$_2$. Unfortunately this dependence in AgGaTe$_2$ is not known, but an analogous behavior of the bandgap has also been observed in other silver containing chalcopyrites like AgGaSe$_2$ and AgGaS$_2$ [53]. In AgInSe$_2$, for example, the bandgap energy increases about 8 meV from $T = 4.2$ K to 150 K [54].

6.3 Photoluminescence of polycrystalline CuGaTe$_2$

CuGaTe$_2$ is a very interesting compound for many reasons. It was found that the complex nature of its pseudo-binary phase diagram leads to the formation of high concentration of intrinsic defects originating from the deviation of its ideal stoichiometry [45, 20]. Therefore a wide range of measured E_g and other

parameters are reported in the literature. At the same time there are indications that a very shallow acceptor with $E_a \approx 1$ meV is present in this compound [32] and this level often leads to the degeneration of the CuGaTe$_2$ samples. Probably these shallow acceptor levels are caused by the high concentration of acceptors in CuGaTe$_2$, see for example [56]. It was shown that the hole gas in CuGaTe$_2$ is degenerate at hole concentrations above 5×10^{18} cm^{-3}, therefore, due to Burstein-Moss shift, higher E_g values are measured using optical absorption [20, 57]. Another interesting fact is the presence of photoluminescence bands at higher energy than the lowest bandgap energy of CuGaTe$_2$ [37, 38, and 39]. It was proposed that lower laying valence bands are responsible for these photoluminescence bands [38]. The highest valence band in CuGaTe$_2$ is characterized by three split bands: Γ_7, Γ_6 and Γ_7. This splitting is the result of the combined effect of crystal field and spin-orbit splitting. However, the valence band structure in CuGaTe$_2$ is not completely understood. Deep photoluminescence bands in CuGaTe$_2$ show properties which are difficult to explain using standard photoluminescence models for deep photoluminescence bands [39]. It was found that the deep photoluminescence band at 0.95 eV shows blue shift with increasing temperature and this shift was explained using the model of spatially curved energy gap [39]. All of these facts indicate that further studies are needed to clarify recombination processes in CuGaTe$_2$. In the present work we study the deep photoluminescence region 0.8-1.3 eV of
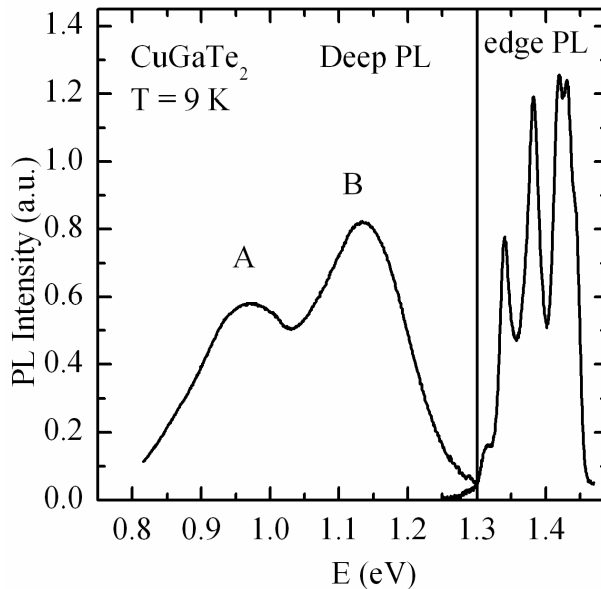

Figure 21a. Photoluminescence spectrum of polycrystalline CuGaTe2 samples. The two regions were recorded with two different detectors. The peaks A and B were located at 0.955 eV and 1.14 eV. The fine structure of edge emission implies that our samples were degenerate.
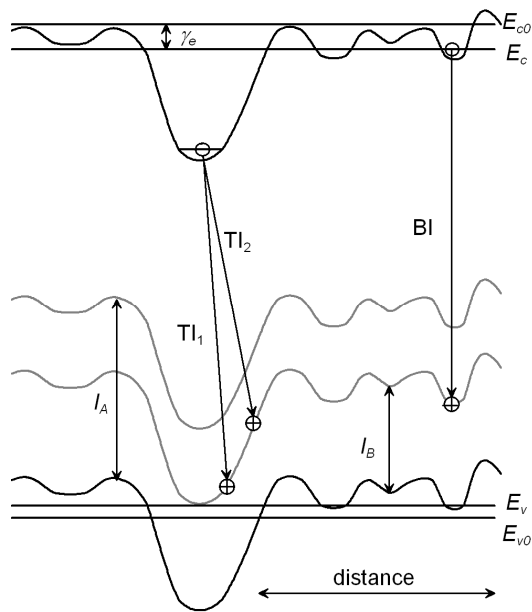
Figure 22. Band diagram of heavily doped semiconductors. I_a and I_b are the defect level binding energies, E_{c0} and E_{v0} are unperturbed edges of energy gap, E_c is the level of free electrons, and E_v is the level of free holes. The BI-band is the result of the recombination of the free electron and the hole that is localized at the acceptor state. Some exceptionally deep potential fluctuations act as potential wells for electrons. Inside those wells, electrons have allowed energy states. From those states electrons can recombine with holes that are localized at acceptor states (TI-band). "Vertical transitions" (TI$_1$) are favoured at higher temperatures while "diagonal transitions" (TI$_2$) are favoured at lower temperatures.

polycrystalline CuGaTe$_2$ samples and present the modernized model of deep level recombination.

The low temperature deep photoluminescence spectrum of our CuGaTe$_2$ samples is presented in Figure 21a. The edge photoluminescence is presented here just to indicate that it exists. The analysis of this part of the spectrum will be presented in the following papers. The deep region consists of two bands. The fittings of these bands showed that they are slightly asymmetrical. The lower intensity band A has the peak at 0.955 eV and the higher intensity band B has the peak at 1.14 eV. This kind of broad asymmetric photoluminescence bands are very common to heavily doped semiconductors. The temperature dependence of the photoluminescence spectra is represented in Figure 24 and the fitting results in Figure 25. Both peaks show a rather significant shift towards higher energies with increasing temperature (40 meV – A peak, 30 meV – B peak). The laser power dependence of the low temperature

photoluminescence spectrum revealed a strong blue shift with increasing excitation power (j-shift) of both bands. Indeed, in the excitation power range from 3 mW to 40 mW, the peaks of A and B bands shifted 10 meV and 5 meV towards higher energies, respectively (see Figure 27).

Because of high concentration of free holes ($>10^{18}$ cm^{-3}), our samples are degenerate. Accordingly, the amplitude of potential fluctuations is strongly reduced by screening. Also, we assume that the effective mass of electrons is small in our samples. Unfortunately, the experimental value of the effective mass of electrons in CuGaTe$_2$ has not been reported in literature. The small effective mass approximation is based on the fact that all chalcopyrite materials tend to have rather small effective masses of electrons [39]. Thus, at the bulk material, there are no potential wells that can trap either electrons or holes. As a result, only exceptionally deep potential wells that are formed by a cluster of defects can localize electrons. Nevertheless, in the presence of deep potential wells, electrons' effective mass is modified as compared to that of the bulk material. The actual value is unknown, but we assume that in our material such exceptionally deep potential wells exist and trap electrons at the present value of their effective mass. The location of those wells is probably some defective area of the crystal lattice. There are several origins that can create this kind of deep quantum wells. The defective spot must either attract donor defects or repel acceptor defects. In both cases there emerges a small volume in the lattice, where the electrons' presence is energetically favorable.

In heavily doped semiconductors the recombination between the conduction band and an impurity level can occur via two channels (see Figure 22). The first so called tail-to-impurity (TI) recombination takes place between the electrons that are localized in the conduction band tails and the holes that are localized at the acceptor state. The second so-called band-to-impurity (BI) recombination takes place between the free electrons in the conduction band and the holes that are localized at the acceptor state.
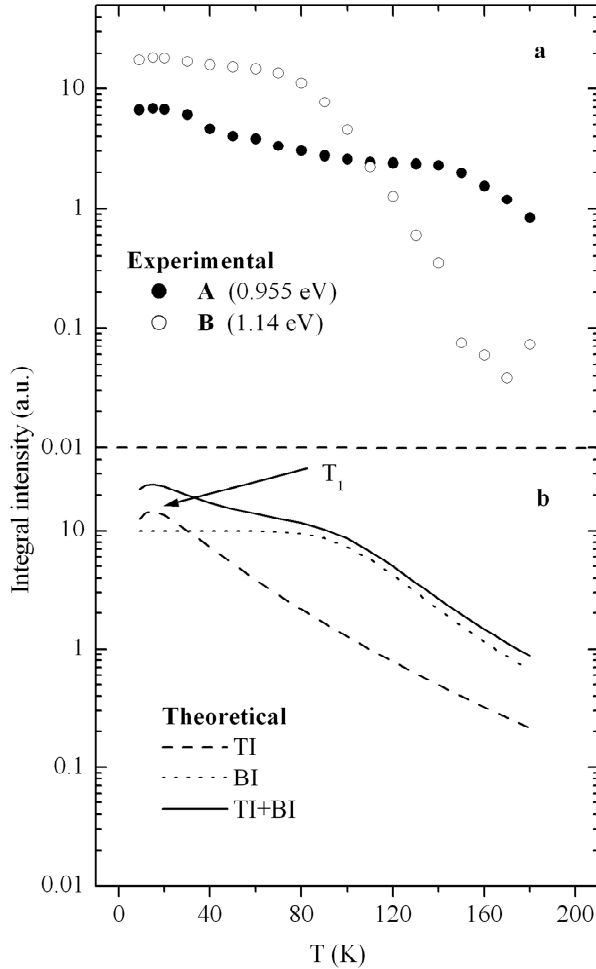
Figure 23. Integral intensities of A and B bands at various temperatures. Upper graph (a) shows the results of fittings of measured photoluminescence spectra. Lower graph (b) shows the theoretical behaviour of TI+BI bands combined. Both bands, A and B, are dominated by TI recombination at low temperatures. At higher temperatures the intensity of TI-band transfers into BI. Integral intensity of TI+BI shows qualitatively very similar behaviour to our measured A and B bands.

Let us now concentrate on the behavior of TI-band. Figure 22 shows that TI-band can exist only if the thermal energy of electrons is not high enough to allow them to escape from the conduction band tails. If not, BI-band can be observed instead of TI-band. Thus, it is expected that as the temperature changes from low to high, TI-band transforms into BI-band. The transition rate depends directly on the depth of the conduction band tails. Thus, the justified

45

question at a given temperature is whether we are observing TI or BI-band. Nevertheless, the TI-band can be easily distinguished from the BI-band. The theory, experiments, and computer simulations in [50] indicate that the maximum of BI-band does not shift according to the laser power variations. On the contrary, the peak position of TI-band should exhibit noticeable j-shift. Namely, because of the localized nature of tail electrons (see Figure 22), TI transition depends on the hole distance from the potential well; arrows TI_1 or TI_2 in Figure 22. Because of the higher energy of the involved holes, the TI_1 recombination results in higher photon energy than the TI_2 recombination. Additional relative energy increase comes from the higher Coulomb term in case of TI_1. Namely, the energy of the emitted photon is increased by the Coulomb term that depends respectively on the distance between recombining charge carriers. By its physical nature the Coulomb term is inversely proportional to the charge separation distance. On the other hand, it is known that because of the lower overlapping of the wavefunctions of distant electrons and holes, the recombination of distant pairs saturates faster than the recombination of close pairs. In conclusion, j-shift in the case of TI-band should be noticeable. Similarly to the donor-acceptor-pair (DAP) recombination, TI-band shifts towards higher energies with increasing excitation power. The thermal quenching of TI-band can be estimated by the expression [46]:

$$I_{TI}(T) \propto \exp[-(kT \ln \Theta + \gamma_e)^{1/2} (4(kT)^{-1/2} + \gamma^{-1/2})] \tag{9}$$

where I_{TI} is the integral intensity, Θ is the factor of excitation level, i.e. the ratio of the density of electronic states to the density of the generated electrons, $\gamma_e = E_{c0} - E_c$ (see Figure 22), E_{c0} is unperturbed bandgap edge, E_c is the level where electrons can be considered as free, and γ is the mean-square fluctuation of the potential energy. The shape of the function (9) is shown in Figure 23b. The intensity of TI-band suffers from both low-, and high-temperature quenching, reaching its maximum value at $kT_1 = (16\gamma_e^2 \gamma / \ln^2 \Theta)^{1/3}$ [46]. The low-temperature quenching is caused by the barrier that holes encounter when physically approaching the potential wells. As a result, at low temperatures the long mean distance between electrons and holes limits the probability of TI recombination. The high-temperature quenching is partially caused by the thermal escape of holes from the impurity level but the main culprit is the thermal liberation of electrons from the conduction band tails. As a result of this process, TI-band simply transforms into the BI-band.

According to [46] the maximum position of TI-band has strong dependence on the temperature. The peak position of TI-band can be calculated as

$$\omega_{\max}^{TI} = E_g^0 - \gamma_e - I_a - kT \ln \Theta + 2\sqrt{(kT)^2 \ln \Theta + kT\gamma_e} \tag{10}$$
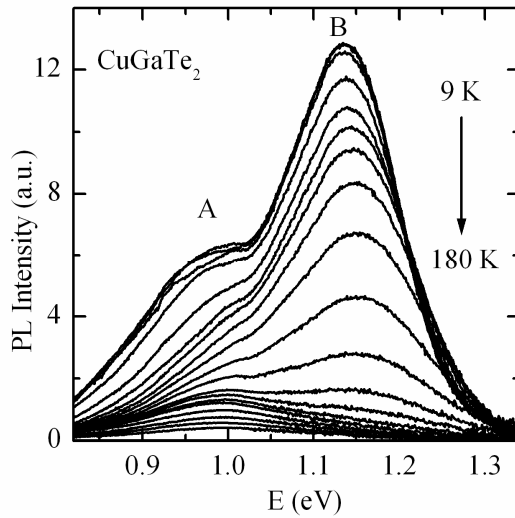
Figure 24. Temperature dependence of deep photoluminescence spectrum of CuGaTe$_2$. Both A and B bands show very similar quenching rates. Both bands exhibit considerable blue shift with increasing temperature (see also Figure 25).
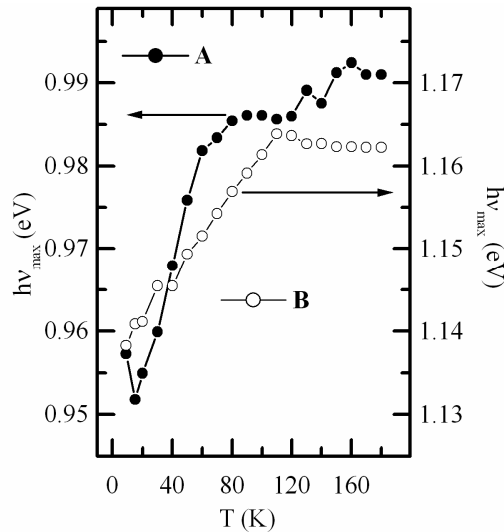

Figure 25. Temperature dependence of A and B peak positions. In the temperature range from 9 K to 180 K the peak position of band A shifts about 40 meV and the peak position of band B shifts about 30 meV towards higher energies.
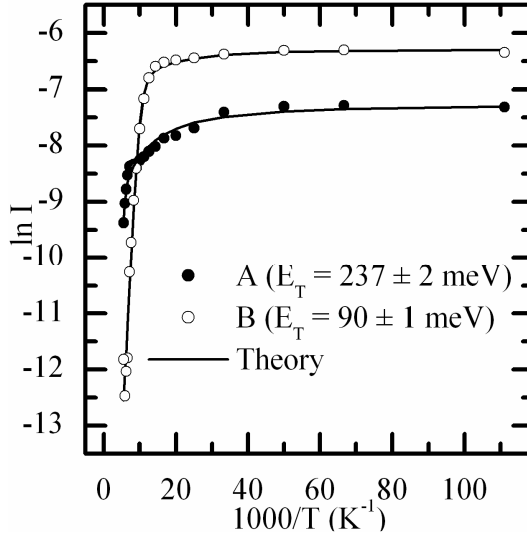
Figure 26. Fitting results of thermal quenching of bands A
and B. The fittings are performed with Eq. (11).

At very low temperatures ($kT < \gamma_e / \ln^2 \Theta$) the maximum of TI-band shifts towards higher energies with the increasing temperature as $\omega_{max}^{TI} \propto 2\sqrt{kT\gamma_e}$. It happens because more TI_1 transitions (see Figure 22) become available as the additional thermal energy helps holes to approach potential wells. At high temperatures and low excitation values ($\Theta \geq 100$) the kT term in Eq. (10) dominates and ω_{max}^{TI} decreases with the temperature increasing. This can be explained as follows. As the temperature increases, the shallower tails are emptied first. As a result, the emphasis of the recombinations shifts to deeper tails which holes find more difficult to approach, consequently, less TI_1 transitions become available.

Figures 24 and 25 show that as the sample temperature increases, the peak position of A and B bands move towards higher energies. At the same temperature range, according to [57], the bandgap energy of CuGaTe$_2$ exhibits the shift in the opposite direction. This implies that both A and B bands comprise two closely situated recombination channels of different origin and the deceptive shift of the peak is actually caused by the transfer of the recombination intensity from one channel to another. We propose that in the present case we see the transition of TI-band into BI-band. However, the involved impurity levels of the A and B bands are different. Accordingly, the activation energies of involved acceptor states are I_A and I_B respectively. Nevertheless, in both cases the shift can be explained as follows. At low temperatures the TI-band, the peak of which is located at slightly lower energy than the BI-band, prevails. As the temperature increases, the photoluminescence intensity transfers from TI-band to BI-band. As a result, although the peaks

48

positions of both TI- and BI-bands are decreasing, the peak position of the resulting band (A or B) is moving towards higher energies.

The temperature dependence of the intensities of A and B bands, also, the TI- and BI-bands inside them are depicted in Figure 23. At low temperatures (below ~30 K) the TI-band prevails. Its intensity has its maximum at the temperature T_1. At higher temperatures the BI-band starts to dominate and the behavior of the A and B bands is governed by the quenching of the corresponding BI-band.

Figure 26 shows the Arrhenius plot of the thermal quenching of the A and B bands. The fittings were performed with the semi empiric equation [38, 39]:

$$\Phi(T) = \frac{I_0}{1 + \alpha_1 T^{1.5} + \alpha_2 T^{1.5} \exp\left(-\dfrac{E_T}{kT}\right)} \;, \tag{11}$$

where $\Phi(T)$ is integral intensity, I_0 is initial intensity, α_1 and α_2 are the process rate parameters, and E_T is the thermal activation energy. The activation energy $E_T^A = 237 \pm 2$ meV of the band A is most probably caused by the thermal activation of holes from the acceptor state I_A directly into the valence zone. In case of band B, the quenching process was detected with the activation energy $E_T^B = 90 \pm 1$ meV. The quenching process is caused by the thermal liberation of holes from I_B acceptor state. These values of the activations energies have not been reported before. At this point, there is not enough information to attribute
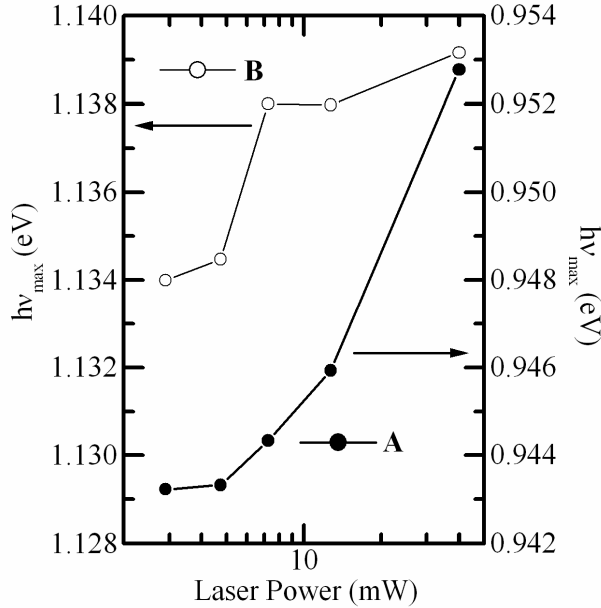

Figure 27. Laser power dependence of the peak positions of photoluminescence bands A and B of CGT. Both bands show rather strong j-shift which is common to TI recombination.

those activation energies to certain defects. The identification of those defects remains for the future studies.

The presence of TI recombination in the bands A and B is confirmed by the laser power dependence of the photoluminescence spectrum (see Figure 27). It was proven in [50] that BI-band does not shift according to excitation power variations. Indeed, the computer simulation showed that the shape and the position of BI-band do not depend on carrier densities. On the contrary, our current experiment showed that at 9 K both A and B bands showed rather strong j-shift. As it was described above, this shift is specific to TI recombination that shifts similarly to DAP recombination.

6.4   Photoluminescence of polycrystalline AgInTe$_2$

The polycrystalline AgInTe$_2$ samples that were made at the Department of Materials Science, Tallinn University of Technology, showed interesting photoluminescence spectra with exciton emission and phonon replicas. The growth procedure was described in Chapter 2. We distinguished three bands that were located at 1.023 eV, 0.959 eV, and 0.741 eV. We assigned the origin of the first band to excitonic emission, the second band to the donor-acceptor-pair recombination.
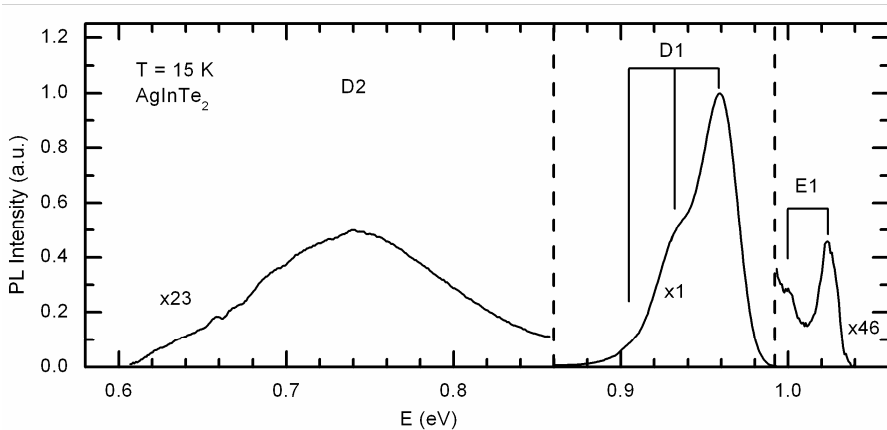
Figure 28. Photoluminescence spectrum of AgInTe$_2$ at 15 K. Different scales are used for different bands. Vertical lines show the positions of the LO-phonon replicas of the E1- and D1-bands. The fitting gave the corresponding phonon energy of $\hbar\omega_{LO}$ = 25 meV.
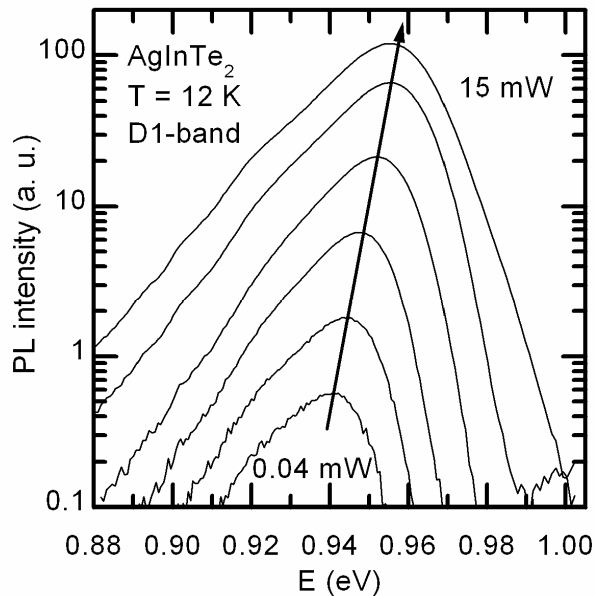

Figure 29. Laser power dependence of the D1-band. In order to avoid the warming of the sample the laser power was varied from 15 mW to 0.04 mW. The rate of the peak position shift is 6 meV per decade.

Figure 30. Temperature dependence of the D1-band. The spectra are normalized.

The typical photoluminescence spectrum of AgInTe$_2$ is shown in Figure 28, where three different photoluminescence bands can be clearly distinguished. The first band (E1) has a relatively narrow peak at 1.023 eV and it has one visible LO-phonon replica with the energy of $\hbar\omega_{LO} = 25$ meV. The second and most intensive band D1 has the main peak at 0.959 eV and it has two LO-phonon replicas with the same phonon energy. The third band D2 is the broadest and is centered approximately at 0.741 eV. Unfortunately, neither the intensity of the E1-band nor the D2-band was high enough to record the

temperature and laser power dependencies. Nevertheless, due to its narrowness we believe that E1 may have an excitonic origin and due to its deepness and broadness D2 is caused by some deep defects.

However, the intensity of the D1-band was sufficient to conduct the measurements of temperature and the laser power dependence. The spectra recorded at various excitation powers from 0.04 mW to 15 mW are shown in Figure 29. As it can be seen, the peak position of the D1-band shifts towards higher energies with the increasing excitation power. The rate of the shift is 6 meV per decade of the laser power. This so called j-shift is characteristic of donor-acceptor pair (DAP) recombination, because at high excitation powers the recombination through distant DAPs saturates. In the case of increasing laser power the recombination rate can only increase through closely situated donors and acceptors which emit photons with higher energies than distant pairs.

In order to obtain information about the energy levels of the involved donor and acceptor states, the thermal quenching of the photoluminescence bands is often used. The temperature dependence of the D1-band in Figure 30 shows the shift of the peak position towards lower energies with the rising temperature. The shift is predominantly influenced by the temperature dependence of the bandgap energy. Indeed, according to [58] the bandgap dependence of $AgInTe_2$ is in the order of -36 meV from 0 K to 300 K. At the same time, the shift of the D1-band in our spectra is about -12 meV from 15 K to 140 K.
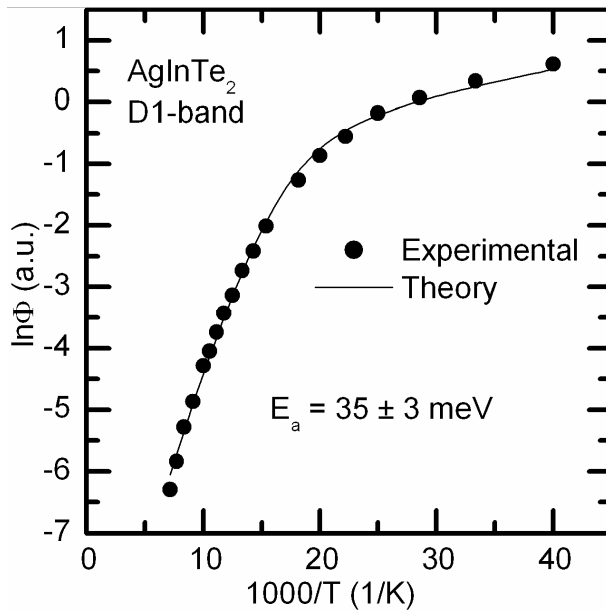

Figure 31. Arrhenius plot of the D1-band. Solid line represents the fitting result using Eq. (11).

According to [59] the thermal quenching of DAP recombination spectrum can be fitted with Eq.(11). The fitting shows (see Figure 31) that the activation energy of the D1-band is 35 meV.

7 Conclusions

The spectrum of the BI recombination in heavily doped single crystalline $CuInTe_2$ has a characteristic asymmetric shape. Also, it features a unique behavior with regard to excitation powers and temperature variations. Our experimental results are in good agreement with the theory of heavily doped semiconductors. Thus, based on the features of the theory, we suggest that the broad band in our spectra was generated by the BI recombination. We attribute the recombination to free electrons with holes that are localized on the acceptor level at 70 meV that is most probably caused by the copper vacancy.

The second $CuInTe_2$ material that was studied was polycrystalline. Our spectra proved that edge and deep photoluminescence bands can be observed in $CuInTe_2$. More work should be done to investigate the origins and possible fine structure of the photoluminescence bands.

The photoluminescence spectra of $AgGaTe_2$ also prove that polycrystalline ternary chalcopyrite materials tend to have large concentration of native defects. This conclusion is based on the observation of the asymmetric shape of the edge emission bands and their temperature dependence. According to the model of heavily doped semiconductors, band-to-band (BB), band-to-tail (BT), and band-to-impurity (BI) bands were identified. From the latter band position an acceptor defect with energy $E_A = 70$ meV was estimated. The bands in the deep photoluminescence region show very rapid thermal quenching with the activation energies about 20 meV. We believe that these bands can be attributed to the deep donor- deep acceptor pair recombination mechanism, but further studies are still needed.

The deep photoluminescence region (0.80 – 1.3 eV) of $CuGaTe_2$ comprises two bands. One of them (at 0.955 eV) has been reported before. The second band (at 1.14 eV) has not been observed before. The similar temperature and laser power dependence of the bands called for similar interpretations. With the increasing temperature we observed the transformation of "tail-to-impurity" (TI) to "band-to-impurity" (BI) recombination. Band A involves the defect level with higher activation energy than band B.

The photoluminescence measurements of polycrystalline $AgInTe_2$ samples showed three bands. Because of the narrowness and closeness to the bandgap energy we assign the first band at 1.023 eV to excitonic emission. The second photoluminescence band at 0.959 eV is assigned to DAP recombination. This conclusion is based on the results of laser power dependence measurements that reveal the j-shift 6 meV per decade. The third photoluminescence band at 0.741 eV is most probably caused by the recombination between deep defect states. However, in order to identify the responsible defects for the E1 and D2 bands, further research is necessary.

8 Acknowledgements

9 References

[1]   Hongsuk Yi, Hyoungwoo Park, J. Korean Physical Society 45 (2004) S530

[2]   G.A.Medvedkin, T.Ishibashi, T.Nishi, K.Hayata, Y.Hasegawa, KI.Sato, Jpn. J Appl. Phys. 39 (2000) L949

[3]   H.Horinaka, N.Yamamoto, Ternary and Multinary Compounds in the 21st Century, IPAP Books 1 (2001) 348

[4]   W.R.L.Lambrecht, S.N.Rashkeev, J.Phys.Chem.Solids 64 (2003) 1615

[5]   K.Tanaka, H.Uchiki, S.Iida, Ternary and Multinary Compounds in the 21st Century, IPAP Books 1 (2001) 296

[6]   N.Kavcar, Solar Energy Materials and Solar Cells 52 (1998) 183

[7]   F.-J.Haug, M.Krejci, H.Zogg, A.N.Tiwari, M.Kirsch, S.Siebentritt, Thin Solid Films 361 (2000) 239

[8]   K.Ramanathan, M.A.Contreras, C.Perkins, S.Asher, F.Hasoon, J.Keane, D.Young, M.J.Romero, W.Metzeger, R.Noufi, J.Ward, A.Duda, Prog. Photovolt. Res. Appl. 11 (2003) 255

[9]   S.F.Chichibu, T.Ohmori, N.Shibata, T.Koyama, T.Onuma, Apll.Phys.Lett. 85 (2004) 4403

[10]   http://isiknowledge.com/

[11]   http://www.sciencedirect.com/

[12]   B.Tell, J.L.Shay, H.M.Kasper, Phys.Rev.B 9 (1974) 5230

[13]   J.E.Jaffe, A.Zunger, Phys.Rev.B 29 (1984) 1882

[14]   L.L. Kazmerski and C.C. Shieh, Thin Solid Films 41 (1977) 35.

[15]   T.Ishizaki, N.Saito, A.Fuwa, Surface and Coatings Tech. 182 (2004) 156

[16]   S.Roy, B.Bhattacharjee, S.N.Kundu, S.Chaudhuri, A.K.Pal, Mat.Chem.Phys. 77 (2002) 365

[17]   I.H.Choi, P.Y.Yu, J.Phys.Chem.Sol. 62 (2001) 825

[18]   C.Rincón, S.M.Wasim, G.Marín, Mat.Lett. 36 (1998) 245

[19]   D.Sridevi, K.V.Reddy, Thin Sol. Films 141 (1986) 157

[20]   G.Marín, G.S.Perez, G.Marcano,S.M.Wasim,C.Rincón, J.Phys.Chem.Sol. 64 (2003) 1869

[21]   M.S,Reddy, K.T.Rreddy, B.S.Naidu, P.J.Reddy, Optical Materials 4 (1995) 787

[22]   T.Bekkay, M.Boustani, K.El Assali, A.Khiara, J.C.Bernede, J.Pouzet, International Journal of Electronics 92 (2005) 445

[23]   W.N.Honeyman, K.H.Wilkinson, J. Phys. D. 4 (1971) 1182

[24]   K.Benchouk, E.Benseddik, C.O.El Moctar, J.C.Bernede, S.Marsillac, J.Pouzet, A.Khellil, European Physical Journal - Applied Physics 10 (2000) 9

[25]   A.Singh, R.K.Bedi, Thin Sol. Films 398 (2001) 427

[26]   U.N.Roy, B.Mekonen, O.O.Adetunji, K.Chattopahhyay, F.Kochari, Y.Cui, A.Burger, J.T.Goldstein, J.Cryst.Growth 241 (2002) 135

[27]   J.L.Shay, J.H.Wernick, Ternary Chalcopyrite Semiconductors: Growth, Electronic Properties, and Applications, Pergamon Press, Oxford, 1975

[28]   C.Rincón, S.M.Wasim, G.Marín, E.Hernandez, J.Galibert, J.Phys.Chem.Sol. 62 (2001) 847

[29]   V.F.Gremenok, I.A.Victorov, I.V.Bodnar, A.E.Hill, R.D.Pilkington, R.D.Tomlinson, M.V.Yakushev, Mat.Lett 35 (1998) 130

[30]   Z.Bahari, J.Rivet, B.Legendre, J.Dugué, Journal of Alloys and Compounds 282 (1999) 164

[31]   E.L.Rogacheva, Cryst.Res.Technol. 31 (1996) S1

[32]   E.I.Rogacheva, Ternary and Multinary Compounds, Proceedings of the 11th International Conference on Ternary and Multinary Compounds, ICTMC-11, Bristol, UK:Institute of Physics Publishing, 152 (1998) 1

[33]   H.Miyake, M.Hibi, K.Sugiyama, and K.Hiramatsu, Jpn. J. Appl. Phys. 39 (2000) 54

[34]   C.Rincón, S.M.Wasim, E.Hernández, and G.Bacquet, Materials Letters 35 (1998) 172

[35]   C.Rincón, S.M.Wasim, G.Marín, G.Sánchez Pérez, and G.Bacquet, J. Appl. Phys. 82 (1997) 4500

[36]   R.Márquez, C.Rincón, Materials Letters 40 (1999) 66

[37]   G. Masse, K. Djessas, L. Yarzhou, J. Appl. Phys. 74, 1376 (1993).

[38]   J.Krustok, H.Collan, K.Hjelt, M.Yakushev, A.E.Hill, R.D.Tomlinson, H.Mändar, H.Neumann, J. Appl. Phys. 83, 7867 (1988)

[39]   J.Krustok, J.Raudoja, M.Yakushev, R.D.Pilkington, H. Collan, J. Appl. Phys. 86, 5305 (1999).

[40]   P.Guha, S.Roy, S.Chaudhuri, and A.K.Pal, Journal of Physics D: Applied Physics, 35 (2002) 1504

[41]   I.V.Bodnar, V.F.Gremenok, R.W.Martin, and M.Yakushev, Solid State Spectroscopy 88 (1999) 424.

[42]   I.V.Bodnar, V.F.Gremenok, R.W.Martin, M.Yakushev, R.D.Pilkington, A.E.Hill, C.A.Faunce, J.A.Berg, O.N.Obraztsova, and R.D.Tomlinson, Jpn. J. Appl. Phys. 39 (2000) 114.

[44]   L.S.Palatnik, E.I.Rogacheva, Sov. Phys. Dokl. 12 (1967) 503

[43]   M.C.Ohmer, J.T. Goldstein, D.E.Zelmon, A.W.Saxler, S.M. Hedge, J.D. Wolf, P.G. Schunemann, T.M.Pollak, J. Appl. Phys. 86 (1999) 94

[45]   E. I. Rogacheva, O. N. Nashchekina, Ternary and Multinary Compounds. Proceedings of the 11th International Conference on Ternary and Multinary Compounds. ICTMC-11. Bristol, UK: Institute of Physics Publishing, p. 159-62. (1998).

[46]   A.P.Levanyuk, V.V.Osipov, Sov. Phys. Usp 24 (1981) 187

[47]   A.Jagomägi, J.Krustok, J.Raudoja, M.Grossberg, and M.Danilson, phys. stat. sol. (b) 237, R3-R5 (2003)

[48]   T.Taguchi, J.Shirafuji, Y.Inuishi, phys. stat. sol. (b) 68, 727 (1975)

[49]   T.Schmidt, K.Lischka, W.Zulehner, Phys. Rev. B 45, 8989 (1992)

[50]   A.Jagomägi, J.Krustok, J.Raudoja, M.Grossberg, M.Danilson, M.Yakushev, Physics B 337 (2003) 369

[51]   J.Krustok, H.Collan, M.Yakushev, and K.Hjelt, Physica Scripta T79 (1999) 179.

[52]   J.Krustok, J.Raudoja, M.Yakushev, R.D.Pilkington, and H.Collan, phys. stat. sol. (a) 173 (1999) 483.

[53]   V.A.Aliyev, G.D.Guseinov, F.I.Mamedov, and L.M.Chapanova, Solid State Communications 59 (1986) 745.

[54]   A.V.Mudryi, I.V.Bodnar, V.F.Gremenok, I.V.Victorov, S.L.Sergeev-Nekrasov, R.D.Tomlinson, A.E.Hill, M.V.Yakushev, amd R.D.Pilkington, Inst. Phys. Conf. Ser. No 152 (1998) 469.

[55]   H.B.Bebb and E.W.Williams, Semiconductors and Semimetals, Vol. 8 Transport and Optical Phenomena pp. 181-420 (1972)

[56]   H.Neumann, D.Peters, B.Schumann, and G. Kühn, phys stat. sol (a), 52, 559 (1979)

[57]   C.Rincón, S. M.Wasim, G.Marín, J. Appl. Phys. 94, 2999 (2003).

[58]   J.Serrano, Ch.Schweitzer, C.T.Lin, K.Reimann, M.Cardona, and D.Fröhlich, Physical Review B, 65 (2002) 125110

[59]   J.Krustok, H.Collan, and K.Hjelt, J.Appl.Phys., 81 (1997) 1442

[60]   B.I.Shklovskij, A.L.Efros, Phys. Semicond. 4, 305 (1970)

10 Curriculum Vitae

Name: Andri Jagomägi
Date of Birth: February 3, 1977
E-mail: andri@kiri.ee
Nationality: Estonian

Employment

Tallinn University of Technology, Dept. of Materials Science, *Tallinn, Estonia,* **Research Scientist** (since January 2002)

DbWeb OÜ, *Tallinn, Estonia,* **Programmer,** (July 2001 - December 2001).

Estonian National Defense Academy, *Tartu, Estonia,* **Physics Lecturer,** (January 2000 - May 2000).

ALL Web Industry, *Tallinn, Estonia,* **Database Designer,** (March 1997 - November 1998).

EETP Ltd., *Tallinn, Estonia,* **AutoCAD Projector**, (1996 November - March 1997).

Education

Tallinn Technical University, *Tallinn, Estonia,* **PhD student**, Engineering Physics, chalcopyrite ternary tellurides, (September 2001 - present)

Master of Natural Sciences, Engineering Physics, (September 1999 – June 2001).

Bachelor of Natural Sciences, Engineering Physics (CUM LAUDE), (September 1995 - June 1999).

University of Sunderland, *Sunderland, United Kingdom*
Visiting student, Nonlinear Dynamics, (January 1998 - February 1998).

Hugo Treffner Gymnasium, *Tartu, Estonia*
Special line of mathematics and physics, (September 1993 - June 1995)

Publications

1. Photoluminescence and Raman spectroscopy of polycrystalline AgInTe$_2$
A.Jagomägi, J.Krustok, J.Raudoja, M.Grossberg, I.Oja, M.Krunks, M.Danilson, *Thin Solid Films*, v. 480-481, p. 246-249 (2005)

2. Device characteristics of CuInSe$_2$ based solar cells
J.Krustok, M.Danilson, **A.Jagomägi**, M.Grossberg, J.Raudoja, *Proc. SPIE* Vol. 5946, p. 236-242, *Optical Materials and Applications;* Arnold Rosental*; Ed.

3. Photoluminescence studies of heavily doped CuInTe$_2$ crystals
A.Jagomägi, J.Krustok, J.Raudoja, M.Grossberg, M.Danilson, M.Yakushev, *Physica B* **337** (2003) 369

4. Deep and edge photoluminescence emission of CuInTe$_2$
A.Jagomägi, J.Krustok, J.Raudoja, M.Grossberg, M.Danilson*, Physica Status Solidi* **237** (2003) R3

5. Monograin layer solar cells
M. Altosaar, **A. Jagomägi**, M. Kauk, M. Krunks, J. Krustok, E. Mellikov, J. Raudoja, T. Varema, *Thin Solid Films* **431** (2003) 466

6. Photoluminescence properties of stoichiometric CuInSe$_2$ crystals
J. Krustok, **A. Jagomägi**, J. Raudoja and M. Altosaar
Solar Energy Materials and Solar Cells **79** (2003) 401

7. Photoluminescence properties of polycrystalline AgGaTe$_2$
J. Krustok, **A. Jagomägi**, M. Grossberg, J. Raudoja, and M. Danilson
Solar Energy Materials and Solar Cells,. v. 90, No. 13, 1973-1982 (2006).

8. Deep defect related photoluminescence in heavily doped CuGaTe$_2$ crystals
A.Jagomägi, J.Krustok, M.Grossberg, M.Danilson, and J.Raudoja, *Physica Status Solidi (a)*, v.203, No. 5, pp. 949-955, (2006).

9. Chemical etching of CuInSe2 absorber surface for monograin layer solar cell application M. Kauk, M. Altosaar, K. Ernits, K. Timmo, **A. Jagomägi**, M. Grossberg, J. Krustok, T. Varema, E. Mellikov., *Proceedings of the 20th European Photovoltaic Solar Energy Conference*, WIP-Munich, Paris, June 2005, pp. 1811-1815 (2006).

11 Elulookirjeldus

Nimi: Andri Jagomägi
Sünniaeg: 3. veebruar 1977
E-mail: andri@kiri.ee
Rahvus: Eestlane

Hariduskäik

Tallinna Tehnikaülikool, *Tallinn*
Doktorantuur, tehniline füüsika, doktoritöö teema "Kalkopüriitsete telluriide fotoluminestsents", (alates september 2001)

Tallinna Tehnikaülikool, *Tallinn*
Loodusteaduste magister, tehniline füüsika, (september 1999 – juuni 2001)

Tallinna Tehnikaülikool, *Tallinn*
Loodusteaduste bakalaureus, tehniline füüsika (CUM LAUDE), (september 1995 – juuni 1999)

Hugo Treffneri Gümnaasium, *Tartu*
Matemaatika-füüsika eriklass, (september 1993 – juuni 1995)

Täiendkoolitused

Loughborough University, Center for Renewable Energy Systems Technology, *Loughborough, Suurbritannia*
Päikesepaneelide testimise süsteemid (jaanuar 2005, 1 kuu)

University of Strathclyde, *Glasgow, Suurbritannia*
Kalkopüriidsete telluriidide luminestsentsi mõõtmine (september 2003 – oktoober 2003)

Uppsala Universitet, *Uppsala, Rootsi*
Kristallide kasvatamise tehnoloogiad (mai 2002, 7 päeva)

University of Sunderland, *Sunderland, Suurbritannia*
Külalisüliõpilane, mittelineaarne dünaamika, (jaanuar 1998 – veebruar 1998)

Töökogemus

Tallinna Tehnikaülikool, materjaliteaduse instituut, pooljuhtmaterjalide tehnoloogia õppetool
Teadur (alates august 2002)
Insener (jaanuar 2002 – august 2002)

Kaitseväe Ühendatud Õppeasutused, *Tartu*
Füüsika lektor, (veebruar 2000 – mai 2000)

ALL Web Industry, *Tallinn*
Andmebaaside disainer, (märts 1997 – november 1998)

AS EETP, *Tallinn*
AutoCAD projekteerija, (november 1996 – märts 1997)

Publikatsioonid

1. Photoluminescence and Raman spectroscopy of polycrystalline $AgInTe_2$
A. Jagomägi, J. Krustok, J. Raudoja, M. Grossberg, I. Oja, M. Krunks, M. Danilson, *Thin Solid Films*, v. 480-481, p. 246-249 (2005)

2. Device characteristics of $CuInSe_2$ based solar cells
J. Krustok, M. Danilson, **A. Jagomägi**, M. Grossberg, J. Raudoja, *Proc. SPIE* Vol. 5946, p. 236-242*, Optical Materials and Applications;* Arnold Rosental*;* Ed.

3. Photoluminescence studies of heavily doped $CuInTe_2$ crystals
A. Jagomägi, J. Krustok, J. Raudoja, M. Grossberg, M. Danilson, M. Yakushev, *Physica B* **337** (2003) 369

4. Deep and edge photoluminescence emission of $CuInTe_2$
A. Jagomägi, J. Krustok, J. Raudoja, M. Grossberg, M. Danilson*, Physica Status Solidi* **237** (2003) R3

5. Monograin layer solar cells
M. Altosaar, **A. Jagomägi**, M. Kauk, M. Krunks, J. Krustok, E. Mellikov, J. Raudoja, T. Varema, *Thin Solid Films* **431** (2003) 466

6. Photoluminescence properties of stoichiometric $CuInSe_2$ crystals
J. Krustok, **A. Jagomägi**, J. Raudoja and M. Altosaar
Solar Energy Materials and Solar Cells **79** (2003) 401

7. Photoluminescence properties of polycrystalline AgGaTe$_2$
J. Krustok, **A. Jagomägi**, M. Grossberg, J. Raudoja, and M. Danilson
Solar Energy Materials and Solar Cells,. v. 90, No. 13, 1973-1982 (2006).

8. Deep defect related photoluminescence in heavily doped CuGaTe$_2$ crystals
A. Jagomägi, J. Krustok, M. Grossberg, M. Danilson, and J. Raudoja,
Physica Status Solidi (a), v.203, No. 5, pp. 949-955, (2006).

9. Chemical etching of CuInSe2 absorber surface for monograin layer solar cell application M. Kauk, M. Altosaar, K. Ernits, K. Timmo, **A. Jagomägi**, M. Grossberg, J. Krustok, T. Varema, E. Mellikov., *Proceedings of the 20th European Photovoltaic Solar Energy Conference*, WIP-Munich, Paris, June 2005, pp. 1811-1815 (2006).

12 Appendix – Papers

A. Jagomägi, J. Krustok, J. Raudoja, M. Grossberg, I. Oja, M. Krunks, M. Danilson, Photoluminescence and Raman spectroscopy of polycrystalline AgInTe$_2$, *Thin Solid Films*, v. 480-481, pp. 246-249 (2005).

Reprinted with permission from Elsevier.

A. Jagomägi, J. Krustok, J. Raudoja, M. Grossberg, M. Danilson, M.Yakushev, Photoluminescence studies of heavily doped CuInTe$_2$ crystals*, Physica B* **337,** pp. 369-374 (2003).

Reprinted with permission from Elsevier.

A. Jagomägi, J. Krustok, J. Raudoja, M. Grossberg, M. Danilson*,* Deep and edge photoluminescence emission of CuInTe$_2$*,, Physica Status Solidi* **237,** R3-R5 (2003).

Reprinted with permission from Wiley-VCH Verlag GmbH & Co KG.

J. Krustok, **A. Jagomägi**, M. Grossberg, J. Raudoja, and M. Danilson, Photoluminescence properties of polycrystalline AgGaTe$_2$*,, Solar Energy Materials and Solar Cells*,. v. 90, No. 13, 1973-1982 (2006).

Reprinted with permission from Elsevier.

A. Jagomägi, J. Krustok, M. Grossberg, M. Danilson, and J. Raudoja, Deep defect related photoluminescence in heavily doped CuGaTe$_2$ crystals*, Physica Status Solidi (a)*, v. 203, No. 5, pp. 949-955, (2006).

Reprinted with permission from Wiley-VCH Verlag GmbH & Co KG.

DISSERTATIONS DEFENDED AT
TALLINN UNIVERSITY OF TECHNOLOGY ON
NATURAL AND EXACT SCIENCES

1. **Olav Kongas**. Nonlinear dynamics in modeling cardiac arrhytmias. 1998.

2. **Kalju Vanatalu**. Optimization of processes of microbial biosynthesis of isotopically labeled biomolecules and their complexes. 1999.

3. **Ahto Buldas**. An algebraic approach to the structure of graphs. 1999.

4. **Monika Drews**. A metabolic study of insect cells in batch and continuous culture: application of chemostat and turbidostat to the production of recombinant proteins. 1999.

5. **Eola Valdre**. Endothelial-specific regulation of vessel formation: role of receptor tyrosine kinases. 2000.

6. **Kalju Lott**. Doping and defect thermodynamic equilibrium in ZnS. 2000.

7. **Reet Koljak**. Novel fatty acid dioxygenases from the corals *Plexaura homomalla* and *Gersemia fruticosa*. 2001.

8. **Anne Paju**. Asymmetric oxidation of prochiral and racemic ketones by using sharpless catalyst. 2001.

9. **Marko Vendelin**. Cardiac mechanoenergetics *in silico*. 2001.

10. **Pearu Peterson**. Multi-soliton interactions and the inverse problem of wave crest. 2001.

11. **Anne Menert**. Microcalorimetry of anaerobic digestion. 2001.

12. **Toomas Tiivel**. The role of the mitochondrial outer membrane in *in vivo* regulation of respiration in normal heart and skeletal muscle cell. 2002.

13. **Olle Hints**. Ordovician scolecodonts of Estonia and neighbouring areas: taxonomy, distribution, palaeoecology, and application. 2002.

14. **Jaak Nõlvak**. Chitinozoan biostratigrapy in the Ordovician of Baltoscandia. 2002.

15. **Liivi Kluge**. On algebraic structure of pre-operads. 2002.

16. **Jaanus Lass**. Biosignal interpretation: Study of cardiac arrhytmias and electromagnetic field effects on human nervous system. 2002.

17. **Janek Peterson**. Synthesis, structural characterization and modification of PAMAM dendrimers. 2002.

18. **Merike Vaher**. Room temperature ionic liquids as background electrolyte additives in capillary electrophoresis. 2002.

19. **Valdek Mikli**. Electron microscopy and image analysis study of powdered hardmetal materials and optoelectronic thin films. 2003.

20. **Mart Viljus**. The microstructure and properties of fine-grained cermets. 2003.

21. **Signe Kask**. Identification and characterization of dairy-related *Lactobacillus*. 2003.

22. **Tiiu-Mai Laht**. Influence of microstructure of the curd on enzymatic and microbiological processes in Swiss-type cheese. 2003.

23. **Anne Kuusksalu**. 2–5A synthetase in the marine sponge *Geodia cydonium*. 2003.

24. **Sergei Bereznev**. Solar cells based on polycristalline copper-indium chalcogenides and conductive polymers. 2003.

25. **Kadri Kriis**. Asymmetric synthesis of C_2-symmetric bimorpholines and their application as chiral ligands in the transfer hydrogenation of aromatic ketones. 2004.

26. **Jekaterina Reut**. Polypyrrole coatings on conducting and insulating substracts. 2004.

27. **Sven Nõmm**. Realization and identification of discrete-time onlinear systems. 2004.

28. **Olga Kijatkina**. Deposition of copper indium disulphide films by chemical spray pyrolysis. 2004.

29. **Gert Tamberg**. On sampling operators defined by Rogosinski, Hann and Blackman windows. 2004.

30. **Monika Übner**. Interaction of humic substances with metal cations. 2004.

31. **Kaarel Adamberg**. Growth characteristics of non-starter lactic acid bacteria from cheese. 2004.

32. **Imre Vallikivi**. Lipase-catalysed reactions of prostaglandins. 2004.

33. **Merike Peld**. Substituted apatites as sorbents for heavy metals. 2005.

34. **Vitali Syritski**. Study of synthesis and redox switching of polypyrrole and poly(3,4-ethylenedioxythiophene) by using *in-situ* techniques. 2004.

35. **Lee Põllumaa**. Evaluation of ecotoxicological effects related to oil shale industry. 2004.

36. **Riina Aav**. Synthesis of 9,11-secosterols intermediates. 2005.

37. **Andres Braunbrück**. Wave interaction in weakly inhomogeneous materials. 2005.

38. **Robert Kitt**. Generalised scale-invariance in financial time series. 2005.

39. **Juss Pavelson**. Mesoscale physical processes and the related impact on the summer nutrient fields and phytoplankton blooms in the western Gulf of Finland. 2005.

40. **Olari Ilison**. Solitons and solitary waves in media with higher order dispersive and nonlinear effects. 2005.

41. **Maksim Säkki**. Intermittency and long-range structurization of heart rate. 2005.

42. **Enli Kiipli**. Modelling seawater chemistry of the East Baltic Basin in the late Ordovician–Early Silurian. 2005.

43. **Igor Golovtsov**. Modification of conductive properties and processability of polyparaphenylene, polypyrrole and polyaniline. 2005.

44. **Katrin Laos**. Interaction between furcellaran and the globular proteins (bovine serum albumin β−lactoglobulin). 2005.

45. **Arvo Mere**. Structural and electrical properties of spray deposited copper indium disulphide films for solar cells. 2006.

46. **Sille Ehala**. Development and application of various on- and off-line analytical methods for the analysis of bioactive compounds. 2006.

47. **Maria Kulp**. Capillary electrophoretic monitoring of biochemical reaction kinetics. 2006.

48. **Anu Aaspõllu.** Proteinases from *Vipera lebetina* snake venom affecting hemostasis. 2006.

49. **Lyudmila Chekulayeva**. Photosensitized inactivation of tumor cells by porphyrins and chlorins. 2006.

50. **Merle Uudsemaa**. Quantum-chemical modeling of solvated first row transition metal ions. 2006.

51. **Tagli Pitsi**. Nutrition situation of pre-school children in Estonia from 1995 to 2004. 2006.

52. **Angela Ivask**. Luminescent recombinant sensor bacteria for the analysis of bioavailable heavy metals. 2006.

53. **Tiina Lõugas**. Study on physico-chemical properties and some bioactive compounds of sea buckthorn (*Hippophae rhamnoides* L.). 2006.

54. **Kaja Kasemets**. Effect of changing environmental conditions on the fermentative growth of Saccharomyces cerevisae S288C: auxo-accelerostat study. 2006.

55. **Ildar Nisamedtinov**. Application of ^{13}C and fluorescence labeling in metabolic studies of Saccharomyces spp. 2006.

56. **Alar Leibak**. On additive generalisation of Voronoï's theory of perfect forms over algebraic number fields. 2006.